Causes of Spinal Injuries in Rear Crashes from the Crash Injury Research and Engineering Network (CIREN)

Chantal S. Parenteau, Rodney W. Rudd, Daniel Camacho

Abstract

This study examines causal factors of spinal injuries in rear-impact crashes. The authors queried the CIREN database and performed an in-depth clinical review of twenty-two belted front-seat occupants who sustained moderate severity spinal injuries in rear-impact crashes.

Thoracic spine fractures were the most common (17), followed by cervical (6) and lumbar (3). Four case subjects sustained fractures in multiple spinal regions and six sustained concomitant spinal cord injuries. The three primary mechanisms identified were spine straightening, fulcrum loading, and buckling resulting from compression. Spine degeneration emerged as a common factor, especially among older occupants in lower severity crashes. Half of the subjects underwent spinal fusion surgery due to the nature of their injury.

The detailed medical findings were crucial in identification of the injury mechanisms and causal factors. Most of the crashes were severe. Most seats exhibited deformation in the field cases examined, even among lower severity impacts, though the role of occupant interaction with the seat structures warrants further examination.

Keywords Spine degeneration, Occupants, Spine injury, Injury databases, Biomechanics / injury prevention for the elderly population.

I. INTRODUCTION

The spine is a key supporting structure of the torso because it routes and protects the spinal cord while providing for flexibility and shock absorption. Motor vehicle crashes are one of the leading causes of spinal injury [1]. Parenteau and Viano [2] analysed US crash data from the National Automotive Sampling System Crashworthiness Data System (NASS-CDS) and reported that spinal cord injury (SCI) occurred in one out of 2,089 front-seat occupants in tow-away rear crashes. Spine injuries may not be the most common injuries in rear crashes but can be debilitating, particularly when they involve injury to the spinal cord [3].

During a rear impact, the vehicle accelerates forward. Consequently, the vehicle floor and seat attachments move forward, displacing the seat forward relative to the occupant. The occupants move rearward relative to the interior due to inertia. The seat is the primary component an occupant engages in a rear crash and it plays a critical role as a restraint. It is designed to support the occupant early in the ride-down phase while maintaining head and torso alignment. Occupant loading is sequential, first with the pelvis, then torso and head, supported by the head restraint. Seats have evolved over time with increased head restraint size. Most first-row seatbacks have a perimeter frame design that allows the occupant to pocket into the relatively deformable middle region while reducing seat-back rotation [4]. Though modern seats are effective in reducing injury [5], injury occurrence in rear impact persists in the field. New injury mechanisms associated with stronger seat-back frames have been reported [6-7].

Various definitions have been used to describe occupant kinematics in rear crashes, including:

- Pocketing: the occupant translates into the central portion of the perimeter-frame seat-back design prior to seat-back rotation.
- Spine straightening: the spine has a natural curvature, including kyphosis in the thoracic spine and lordosis in the lumbar area. The spine can straighten against the seat back during the initial loading early in the crash sequence before seatback deflection occurs [4].
- Ramping: occupants can slide along and translate up the seat backrest. Ramping is the translational displacement of the lower torso along the seat back of at least 7.5 cm [8]. It has been observed at maximum deflection in very high-speed rear crashes or when the seat-back rotation becomes limited. Ramping can also occur with vehicle over-ride [9].

Figure 1 provides an illustration of some terminologies used to describe occupant kinematics in rear crashes.

Dr C. S. Parenteau (e-mail: cparenteau@dreng.com; tel: +1-248-339-6700) is an Engineering Consultant at Design Research Engineering, USA; Dr. R. Rudd (e-mail: rodney.rudd@dot.gov; tel: +1-434-242-4950) is a Senior General Engineer at the National Highway Traffic Safety Administration, USA; Dr. D. Camacho (e-mail: danielcamachomd@gmail.com; tel: +1-920-257-9014) is a Neuroradiologist and Biomechanical Engineer at Camacho Consulting, USA.

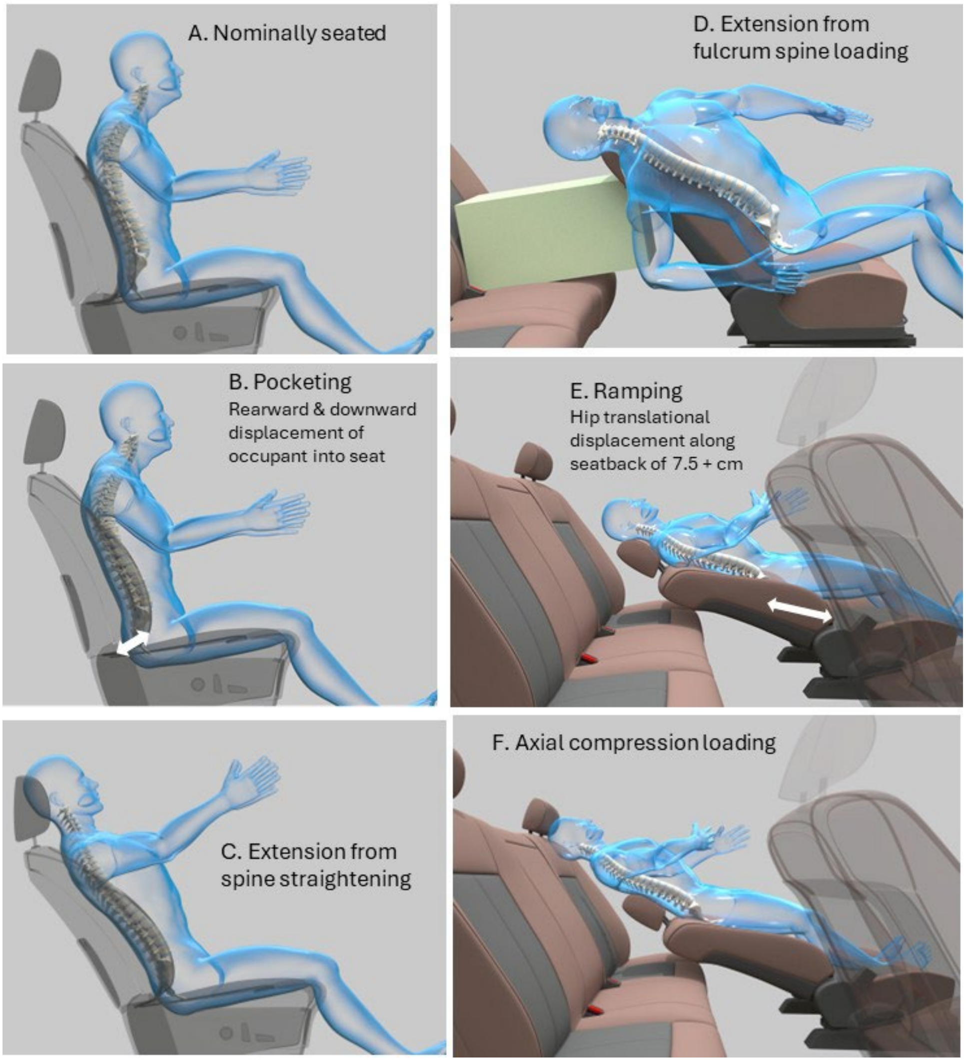

Fig. 1. Occupant kinematics in a rear impact. Panel A depicts a nominally-seated occupant with a typical seat configuration. Panel B shows the torso moving into the seat back (pocketing) during the initial loading. Panel C depicts the straightening of the upper thoracic spine as the inertia of the head leads to delayed engagement with the head restraint. Panel D shows a condition where the upper torso and head are unsupported due to oblique loading such that a fulcrum-type loading occurs in the thoracic spine as the torso hinges on the inboard seat frame. Panel E shows an occupant who has ramped up the seatback, and Panel F shows the head contact to an interior structure to produce a compressive load in the spine.

Primary Spine Injury Scenarios in Rear Crashes

Extension During Spine-straightening

Spine straightening occurs when the kyphotic curvature of the thoracic spine is straightened along the seat back as the occupant moves rearward relative to the vehicle interior and prior to much seatback rotation. Viano *et al.* [8] presented four field incidents where thoracic spinal fractures coincided with spine straightening. All four occupants had calcification across the intervertebral joints from a pre-existing ankylosing spinal disorder, a degenerative condition that stiffened the spine. When a motor vehicle occupant with an ankylosing spinal disorder – such as Diffuse Idiopathic Skeletal Hyperostosis (DISH), Ankylosing Spondylitis (AS), and/or Degenerative Spondylosis (DS) – sustains the forces imparted in a rear-impact collision, the forward acceleration of the occupant by the seat backrest attempts to straighten the kyphotic curvature of the thoracic spine, as the head and upper torso move rearward relative to the vehicle interior [6-7][11]. While a normally flexible thoracic spine would straighten by extending over multiple intervertebral joints along the full length of the thoracic spine to distribute loads broadly over the spine and seat back, a stiffened thoracic spine is less able to straighten/extend, creating greater potential for extension-type fracture-dislocations [6-7][11]. These extension injuries can occur without the occupant ramping up the seat backrest or moving off the support from the seat back and head restraint [6]. Increased seat backrest stiffness, which increases torso acceleration and the inertial extension moment on the thoracic spine, can exacerbate this injury mechanism [7]. Panel C in Figure 1 provides an illustration of spine straightening.

Extension from Fulcrum Loading

Impact-induced yaw motion or angular trajectory of the vehicle can cause the occupant to move at an oblique angle with respect to the longitudinal axis of the vehicle and seat back. This can lead to the occupant's upper body moving laterally off the seat back. Viano *et al*. [10] discussed four field cases where the thoracic spine was injured when the head and upper body moved inboard or outboard of the head restraint and seat frame, resulting in fulcrum loading [10]. Severe retrolisthesis was observed.

The effect of fulcrum loading has been studied in laboratory settings [8-9]. For example, Viano et al. [10] conducted a series of 56 km/h rear sled tests with a 95th percentile Hybrid III lap-shoulder-belted anthropomorphic test device (ATD) in an All-Belt-to-Seat (ABTS) condition. In one test, the ATD was leaned inboard and in the other, inboard and forward. The neck extension moment was 143% of injury reference value in the case with inboard and forward positioning. Fulcrum loading occurred because the upper body was not supported by the seat and head restraint due to initial posture of the ATD and/or oblique loading. Fulcrum loading was also observed in a very high-speed rear impact sled test (56 km/h) with a rigidized seat back, while the head and neck continued to load the unsupported head restraint [12]. Panel D in Figure 1 provides an illustration of fulcrum loading.

Axial Compression with Buckling and Localised Bending

Axial compressive spinal injuries can occur when the front-seat occupant moves head-first into the roof or second-row area. Parenteau and Viano [13] conducted an in-depth review of electronic NASS-CDS cases involving front-seat occupants with serious-to-maximal (AIS3–6) spine injury involved in a rear impact. They reported on three cases where the occupants were injured by impacts into the rear seat backrest, resulting in spinal injury. These injuries generally result from the forces applied to the spine when the head and/or upper torso interact with the roof or rear seat backrest, and the cervical and upper thoracic spine sustain compressive loads between the lower torso and the head/shoulders. The compressive load applied along the spine's inferior-superior axis leads to spinal buckling, which can superimpose localized bending and compression at the motion segments. These kinematics have been reported in laboratory settings involving high-speed rear-end sled tests, but those tests were conducted with vintage seats [14]. Panel F in Figure 1 provides an illustration of axial compression which can lead to buckling with localised bending.

Factors Influencing Injury Outcome

Various factors can influence the injury outcome including the following:

Crash Severity

Injury risk increases with crash severity [15]. Crash severity is often discussed in terms of the change in speed experienced by the vehicle during the impact – the delta V. The distribution of tow-away rear crashes has been assessed by crash severity, where the 50th percentile delta V corresponded to 18.5 km/h for all exposed and 34.5 km/h for seriously (Maximum Abbreviated Injury Scale, MAIS3+) injured [16]. The average delta V in US Federal Motor Vehicle Safety Standard (FMVSS) 301R tests ranged from 30.4 km/h for pickups to 38.6 km/h for passenger cars, consistent with the 50th percentile delta V for serious injury [17].

Rear crashes with a 24 km/h or lower delta V are considered "low-to-moderate" in severity and account for more than 70% of all tow-away crashes [18]. Viano and Parenteau [19] reviewed individual cases with a seriously injured driver in delta Vs up to 24 km/h and observed that most involved older occupants and/or those with spine degeneration. In a study of contemporary US field cases, Lockerby and Rudd found delta V to be a significant predictor of AIS2+ cervical and thoracic spine injury [20].

Intrusion

Viano and Parenteau [19] analysed field accidents and found that intrusion can be significant in 56+ km/h rear impacts. Intrusion has been shown to occur early in laboratory rear crash tests. For example, Parenteau *et al.* [21] evaluated the response of front-seat ATDs in deformable barrier tests at 80 km/h and 70% offset. The authors reported that intrusion occurred early in the collision before much movement of the occupant or seat back. Intrusion can push, support, and rigidise the front seats, affecting loading and occupant kinematics.

Occupant Size

Parenteau *et al*. [22] reviewed rear sled data and quantified how occupant weight can increase seat-back rotation. Edwards *et al.* [23] analysed field crash data and reported that obese occupants had a significantly higher risk of severe injury than normal BMI (Body Mass Index) front-seat occupants in rear crashes. Seat-belt routing and fit differ in obese compared to normal BMI occupants due to increase in body dimensions and belt webbing length, as previously discussed in [22]. Weight can be a factor in the injury outcome since it increases inertial loading, particularly in fulcrum loading scenarios [8][10]. Weight can also affect the centre of gravity, and thus the moment arm of loading to the seat backrest. For example, Viano *et al.* [10] observed if the head-neck and upper torso are misaligned with the head restraint, either due to inboard or outboard posture and/or impact direction, the spine can experience inertial forces as the unsupported mass continue to accelerate. This response is common when the seat back remains upright and rigidised. The authors reported that forces resulting from fulcrum loading are likely greater with heavier occupants, and the size and strength of the spine does not proportionately increase with higher body mass.

Rebound

Rebound is the forward occupant excursion resulting from stored seat energy. It usually occurs after maximum seat-back deflection. Rebound results in a relative forward velocity for the occupant within the vehicle interior compartment. Galli and Digges [24] noted that unrestrained occupants could sustain injuries during rebound from secondary impacts with the front interior. A rear impact event may also be followed by a frontal crash event, which introduces an additional source of energy affecting kinematics and injury outcome [25]. In multiple-impact crashes, it may be difficult for crash investigators to assign injury sources and mechanisms.

Objects in the Rear

Viano and Parenteau [19] reviewed FMVSS 301 tests with instrumented dummies. Objects behind the front seats interacted with seat-back rotation and loaded the occupant. This led to an increase in some front-occupant responses, particularly in the chest acceleration in some tests. Objects in the second row, such as cargo or a child restraint seat, can limit seat-back rotation and be a cause of concentrated loading on the first-row backrest and occupant. Parenteau *et al.* [9] discussed a severe crash test with override and intrusion which involved an unbelted ATD in the driver seat. They observed that the impact force caused the ATD to move rearward and load the driver's seat back, which rotated until its movement was arrested by interaction with the rigidised support structure. The ATD then ramped up the supported seat back and the head impacted the simultaneously deforming roof panel.

Spine Degeneration

The association between increased risk of spine injury risks and spine degeneration has been discussed [6-7][26]. In rear impacts, the types of degenerative spine disease most frequently discussed are those that increase spine stiffness. These include DISH, AS, and DS. DISH is a disorder characterised by excess bone formation and continuous ossification of soft tissue structures along the anterior and lateral aspects of the spine, generally with preservation of intervertebral disc height and apophyseal joints. In AS, autoimmune-mediated inflammation results in new bone formation bridging the intervertebral disc spaces, facet joints, and sacroiliac joints. DS primarily affects the intervertebral disc spaces, uncovertebral joints, and facet joints, and results in a loss of joint space, joint surface irregularity, and reactive osteoarthritic hypertrophy. It results in osteophyte formation which can bridge and fuse the intervertebral joints.

In degenerative diseases causing pathological spinal stiffening — including DISH, AS, and DS — the stiffened spinal segments lose normal viscoelastic energy dissipation and create longer mechanical lever arms, rendering them structurally brittle and vulnerable to fracture even from minor trauma, both within the fused segments and at adjacent mobile segments [27-29]. Importantly, this elevated fracture risk is independent of bone mineral density [29-31]. Other types of spine degeneration can also influence injury outcome, including hyperkyphosis, osteoporosis, and stenosis [19][26]. Kyphosis generally refers to a convex curvature of the spine in the sagittal plane. A diagnosis of hyperkyphosis typically refers to excessive kyphosis of the thoracic spine. Osteoporosis results from a chronic imbalance between rates of bone resorption and bone deposition. A decrease in bone mineral density results in lower fracture tolerance. Stenosis refers to narrowing of the spinal canal or neural foramina. Stenosis is most often degenerative but can also be congenital. Stenosis can increase the risk of neurological injuries in traumatic events [32]. It should be noted that age is often associated with spine degeneration as degenerative changes develop over time. The increased prevalence of degenerative spine pathology with age is well documented [33-37].

Need for Radiology

Radiological evaluation is fundamental to the reconstruction of spinal injury mechanisms following rear-impact trauma, as characteristic patterns identified on computed tomography (CT) and magnetic resonance imaging (MRI) enable correlation between underlying imaging findings and injury classifications, including compression injuries (AO type A), distraction injuries (AO type B) and displacement/translational injuries (AO Type C). Distinct "fingerprints" on CT – such as vertebral body wedging, burst fracture with retropulsion, or translational malalignment – have been shown to correspond reliably to specific biomechanical loading vectors [38-39]. MRI complements these findings by sensitively depicting bone marrow edema, ligamentous disruption, intervertebral disc injury, spinal cord pathology, and paraspinal soft tissue injury, thereby refining assessment of instability and distinguishing between compression, distraction, and combined loading mechanisms [40]. The integration of CT-defined osseous injury patterns complemented by MRI-demonstrated bone marrow, soft tissue, and ligamentous injury provides a comprehensive, mechanism-based framework through which the magnitude, direction, and sequence of forces imparted to the spine may be deduced with a high degree of specificity.

Objective

The objective of this study was to identify characteristics, mechanisms, and causal factors of spinal injuries to belted occupants in rear-impact crashes through in-depth review of crash and medical data from field crashes. The observations are intended to enhance assessment of crash injuries and exploration of injury countermeasures, as well as educate on post-crash care considerations.

II. METHODS

Database

The National Highway Traffic Safety Administration (NHTSA) operates three investigation-based field crash data collection programs. One is the Crash Injury Research and Engineering Network (CIREN), which combines extensive data collection with professional multi-disciplinary analysis of medical and engineering evidence to determine injury causation [41]. CIREN cases are initiated from an injured case subject at the treating trauma centre. The CIREN program is unique in that it augments detailed crash and injury data with additional medical information, including medical imaging. CIREN cases typically include digital radiology as supporting documentation for injury and causation assessment, and the radiology is stored and available for research use. The CIREN process does not influence medical care and CIREN centres can only collect the imaging performed for the case subject's acute care. Procedural limitations may affect the extent of imaging that is stored in the database for some cases.

CIREN collects approximately 180 cases per year in a purposive sample, with 1,160 total cases available from the data collection period considered in this study (2017–2025). The CIREN cases include vehicle and scene information collected using standard NHTSA field crash investigation protocols. Injury causation is documented using the BioTab methodology [42]. CIREN cases undergo a multi-disciplinary deliberative review process to assign injury causation scenarios. Following a quality control process and NHTSA approval, CIREN case data are available for public inspection via an internet-based case viewer: [https://crashviewer.nhtsa.dot.gov/ciren/searchindex].

Rear impacts in CIREN were defined using the damage plane (CDCPLANE) for the vehicle's most significant event (DVRANK=1) with principal directions of force between 140° and 220°. Vehicles experiencing a rollover event were excluded. Passenger cars, utility vehicles, minivans, and pickup trucks were included in the analysis.

Front-outboard occupants 15 years and older were included. This study was limited to 3-point lap- and shoulder-belted (BELTUSE=4) and non-ejected (EJECTTYPE=0) occupants. Injury severity of the occupant was assessed using the Abbreviated Injury Scale (AIS) [43]. Spine injuries were defined using the AIS body region (REGION = 6) variable. Spine region (cervical, thoracic, or lumbar) was identified using the STRUSPEC variable (fourth position of AIS code). Injury severity included moderate (2) to maximal (6) for this study.

The reported impact severity for the event (delta V) was calculated using WinSMASH. For the cases with unknown delta V, the EDR data were used. A crash severity of 56 km/h or higher is considered very severe, as it accounts for less than 0.5% of tow-away rear crashes [44].

Additional assessments

Unique analysis characteristics used in this study are derived by the authors from CIREN data and radiology, including

Energy Transfer to the Seat

In a rear impact, the seat provides an interface and limits the energy transferred to the occupant by yielding. The amount of energy that is transferred to the occupant as the seat back deforms depends on crash severity and occupant mass. The amount of energy can be approximated by $E = ½*0.65*m(\Delta V)^2$ using 65% of the occupant mass (m) and delta V [22]. For example, in a 40 km/h rear sled test with a 50th Hybrid III ATD, the estimated energy transfer to the seat would be 3,150 J ($1/2*65\%*78.2\ kg*(40\ km/h)^2$) [16]. The energy transfer to the seat in FMVSS 301 rear crash tests is about 2,922 J for passenger cars, 2,527 J in utility vehicles, 1,812 J in pickups, and 2,361 J in minivans [17]. The energy transfer to a seat is about 4,708 J in 49 km/h rear sled tests with the 50th Hybrid III [45].

Comorbidities assessed from radiology

The presence of pre-existing spinal comorbidities was established by direct evaluation of the available radiological imaging studies.

- DISH: The criteria of Resnick and Niwayama [46] determined the presence of DISH.
- AS: The Assessment of Spondylarthritis International Society (ASAS) classification criteria (imaging arm) established the diagnosis of Ankylosing Spondylitis [47].
- DS: Degenerative Spondylosis was diagnosed by the presence of facet degeneration and/or disc degeneration using the grading schemata of Park *et al.* [48], Liebsch *et al.* [49], and Liebsch *et al.* [50].
- Osteoporosis: Osteoporosis was defined as mean Hounsfield Units (HU) <130 within the L1 vertebral body [51].
- Stenosis: Spinal canal stenosis was defined as Torg Ratio <0.7 in the cervical spine [52], and anteroposterior spinal canal diameter less than two standard deviations below the mean canal diameter at the closest uninjured thoracic spinal level reported by Scoles *et al.* [53].
- Kyphosis: Thoracic spinal kyphosis was defined as T2-T12 Cobb angle measurement more than two standard deviations greater than the mean angle of the age- and sex-matched group reported in Fon *et al.* [54].

See Appendix D for more information and visual examples of different types of spine degeneration.

Analysis

In this study, the CIREN cases were first analysed to determine the distribution of crash circumstances and injuries by spine regions. The available radiology studies were reviewed with a board-certified neuroradiologist to assess the loading patterns revealed by the imaging findings as well as to identify the presence of pre-existing spinal comorbidities noted above. The results were combined with the crash circumstance and occupant kinematics data to identify the spine injury mechanisms and potential related contributing factors.

III. RESULTS

Crash Circumstances

The selected cases included 20 rear-impact crashes with 22 occupants who sustained moderate to critical spine injuries. Appendix A includes details on the vehicles and crashes. It provides a summary of the vehicle information, including the characteristics of the (highest severity) rear impact as well as overall number of crash events for the subject vehicle. The model years ranged from 2009 to 2024, all complying with the FMVSS 301 upgrade and FMVSS 202a. Appendix A also includes an indication of factors, including excessive speed with a delta V of 56 km/h and above, multiple events, and whether the crash direction was oblique (15 deg. or more from pure rear). Of the 22 occupants, 12 were exposed to a rear impact with excessive speed, 14 to multiple impacts, and two to oblique impacts.

Appendix B lists the occupant information. The average age, height, and weight of the 22 belted and non-ejected front-seat occupants with moderate-to-critical spine injuries were 61.2 ± 11.8 years, 173.6 ± 10.1 cm, and 99.8 ± 20.1 kg. The energy transfer to the seat was estimated using occupant weight and delta V information. Figure 2 shows the results with more than half of the CIREN cases evaluated having an energy of 5,500 J or greater, highlighting the severity of the crash conditions in this subset of cases. Energy to the seat of 5,500 J or higher is considered exceedingly severe. Energy of 5,500 J represents a rear impact resulting in a 53 km/h delta V with a 50th Hybrid III ATD.

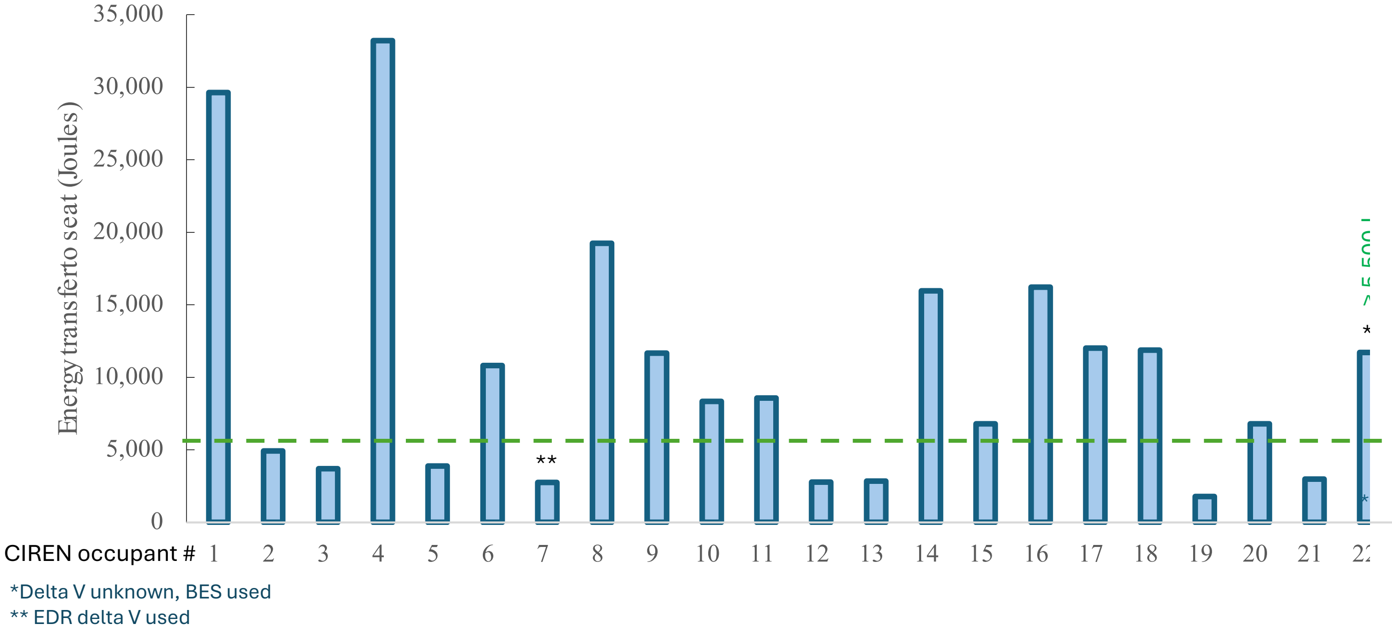

Fig. 2. Estimated energy transfer to the seat in the CIREN cases.

In-depth Case Review

Injury Distribution

The spine injuries are summarised in Appendix C, with additional case detail and graphics provided in Appendix E. There were two occupants who had spine injuries in both the cervical and thoracic spine, and two who sustained thoracic and lumbar spine injuries. The total number of affected spine regions in this study is 26. The left-side chart of Fig. 3 shows the distribution of affected spine regions: 23% in the cervical spine, 65% in the thoracic spine, and 12% in the lumbar spine.

In some cases, the same vertebra sustained multiple fractures, which are coded in a combined manner based on AIS rules. Most of the injuries were fractures, but there were six spinal cord injuries in conjunction with fractures or dislocations. Rib fractures were observed in 14 occupants. The right-side chart of Fig. 3 shows the distribution of the AIS-coded injuries by spine regions. Of the 39 AIS2+ coded spine injuries, 25% were in the cervical spine, 67% in the thoracic spine, and 8% in the lumbar spine. It should be noted that some spine injuries were in the same area and occurred at the same time in the crash sequence, from the same loading mechanisms. The results indicated that most occupants had more than one moderate-to-critical (AIS2-5) spine injury (39 injuries in 22 occupants). Half of the case subjects underwent a fusion surgery, seven were placed in a brace or collar, two cases showed no documentation of a treatment, and one was a fatality.

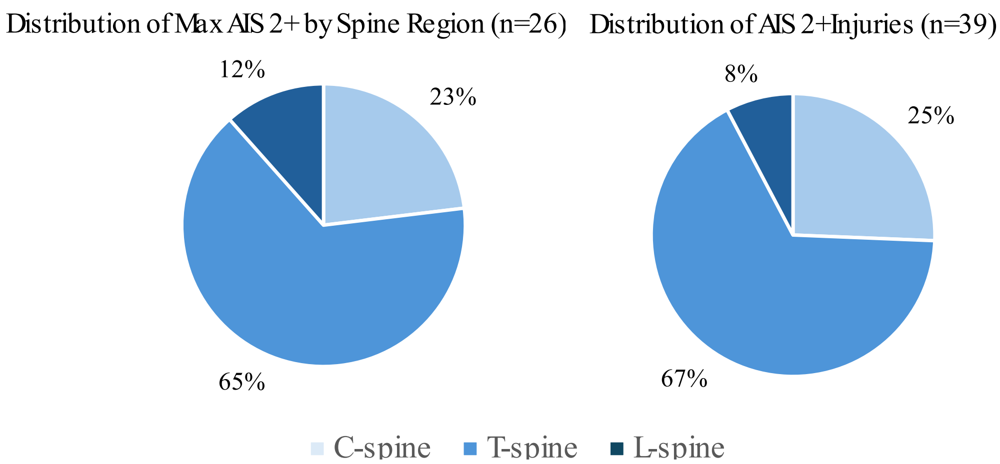

Fig. 3. Distribution of moderate and higher (AIS2-6) spinal injuries in non-ejected and belted front-seat occupants involved in rear crashes by spine region from CIREN.

Injury Mechanisms

The injury mechanisms are tabulated in Appendix C and Appendix E includes additional information on the occupant kinematics, spine injuries, and associated mechanisms. Of the 22 occupants analysed, there were 39 AIS2+ spine injuries coded. Some injuries were coded at the same vertebral area. Only one injury mechanism was listed for the group of injuries at the same vertebral area. For example, the occupant in case 22 was diagnosed with a T12 vertebral fracture (AIS4) and multiple fractures of the T11, including the transverse process, spinous process, and vertebral body (AIS2). These two injuries all resulted from the same mechanism in the lower thoracic spine. However, some spinal injuries occurred at distant vertebral locations for four of the cases (Cases 7, 11, 19, and 20). The occupant in case 11 was diagnosed with a T3 vertebral body minor compression fracture (AIS2), a T9 bilateral facet fracture (AIS3), and a combination of injuries at the T10 vertebral level, including bilateral facet fractures (AIS3), vertebral body minor compression (AIS2), and disc herniation (AIS2). The injury mechanisms were different at T3 from those at the T9-T10 area. Similarly, the occupant in case 20 was diagnosed with a C7 vertebral fracture (AIS3), a T1 vertebral fracture (AIS2), and two T11 vertebral fractures (AIS2-3). The injury mechanisms were different at C7-T1 from those at the T11 area. Of note, some occupants were exposed to various loadings due to the complexity of rear crashes. Only the initial mechanism was reported as the loading causing the fracture. It is possible that the additional loading may have exacerbated the outcome.

Overall, of the 22 occupants with moderate-to-critical spine injuries, there were 24 spine areas with specific injury mechanisms. These included:

- Extension loading: the in-depth case review indicated that 13 of the 24 spine areas with AIS2+ spine injuries were from extension. Extension occurred when the kyphotic spine segments attempted to straighten along the seat back with the occupant relatively upright in the seat It should be noted that all these involved pre-existing calcification and spinal degeneration that stiffened the spine and lowered the tolerance.
- Axial compression with buckling and localised bending: six of the 24 injured spine areas resulted from the head contacting a vehicle structure with inertial loading from the torso. For example, case 4 involved cargo in the 2nd row area that limited the seat-back rotation and redirected the occupant kinematics. The injuries occurred from initial compression from head contact, followed by localised spinal column buckling and flexion. Possible belt misrouting was noted in one case (case 9) based on the bruising pattern on the chest-abdominal area, which was consistent with an abnormally caudally positioned shoulder belt. The occupant's spinal injuries likely occurred during rebound and/or subsequent frontal impact, when the upper torso flexed over the low-positioned shoulder belt. Of note, except for one case, all involved spine degeneration.
- Tension with extension: spine tension with some extension was observed in two of the cases. This type of mechanism is often associated with fulcrum loading. Hyper-extension occurred when the upper torso moved off the seat back while it was upright. The spine hinged rearward around the seat-back frame.

Spine Comorbidities

In addition to the MRI and CT imaging, the radiology reports and additional findings from the CIREN radiologists were also available. The results were used to identify the type of spine degeneration. Appendix E includes commentary and images depicting the spine degeneration identified from the radiology records. Table DI in Appendix D provides a summary for the 22 subjects examined in this study. Spine degeneration was documented or observed in 18 of the cases. The prevalence was 81% (17/21) for spine stiffening (DISH, AS, or DS), 41% for osteoporosis (7/17), 31% (5/16) for hyperkyphosis, and 32% (6/19) for stenosis. The radiology review identified all the comorbidities were localised at the level of spine injury, in particular ones that result in stiff and brittle joints, such as DISH and Degenerative Spondylosis. This increased the likelihood of fracture during straightening of the spine.

IV. DISCUSSION

In this study, field crashes were reviewed to evaluate spine injuries to lap-shoulder-belted front-seat occupants involved in a rear impact. The rear impact was the most severe event and vehicles experiencing a rollover were excluded. The CIREN database was selected as it provides a unique opportunity to analyse crash circumstances, restraint performance, occupant characteristics, detailed medical history, injury details and associated mechanism, and radiology findings.

Occupant Size and Age

On average, the occupants involved in this study were 61.2 ±11.8 years old and weighed 99.8 ±20.1 kg. Parenteau *et al.* [17] analysed NASS-CDS and Crash Investigation Sampling System (CISS) data and determined that the average driver was 36.4 years old and 76.4 kg, and the average right-front passenger was 30.5 years old and 67.8 kg. This highlights an important feature of the CIREN case subjects examined in this study, who are older and heavier than the averages of exposed occupants.

Injury Distribution

Parenteau and Viano [2] evaluated 1994-2011 NASS-CDS data using tow-away vehicles with a 1994+ model year and reported that serious (AIS3+) spine injuries were equally distributed to the cervical and thoracic area in rear crashes. Serious (AIS3+) injuries to the lumbar area were uncommon. This study was conducted with more recent data and with modern vehicles (model year 2009-2024). The front seats included were designed to meet new head restraint requirements, Insurance Institute for Highway Safety (IIHS, new evaluation program, terminated in 2022), and FMVSS 202a. Most injuries (67%) were in the thoracic spine. Only 25% were in the cervical spine and 8% in the lumbar. This change in distribution suggests that newer seats may have become more effective in protecting the cervical spine. Risks of injury cannot be assessed using CIREN data, but this finding warrants an investigation of statistically representative field data to assess whether newer vehicle designs have led to similar changes more broadly. Since the crashes in this study were generally more severe and involving older occupants with pre-existing spinal conditions, any subsequent analysis of field data should examine influence of age and crash severity on the distribution and type of injuries.

Crash Severity

The average delta V in this cohort of cases was 60.2 ± 27.2 km/h, highlighting the generally high severity of the cases reviewed. Of the 22 occupants, 12 were exposed to a rear impact with excessive speed. Parenteau *et al.* [4] reported that the 50th percentile delta V was 18.5 km/h for exposed drivers in tow-away rear crashes. The corresponding delta V was 34.5 km/h for serious injury (MAIS3+).

In two cases examined in this study, the intrusion supported the seat upright or pushed it forward. In two other cases, the seat was supported by objects in the 2nd row area. Edwards *et al*. [23] reported that non-rotated seat back increased severe injury risks by 3.8-times for front-seat occupants in 48+ km/h delta V rear crashes.

Twelve of the 22 cases involved more than one impact. The loading to the spine becomes complex due to multiple loading events. Most of the spine injuries observed in this study occurred early in the crash sequence, generally during the initial spine straightening. However, the additional loading events may have exacerbated the injury outcome. Injury risks are higher in multi-impact crashes than in single event crashes [25]. Digges and Bahouth [55] showed that the rate of serious injury was higher in crashes with two or three or more impacts than in a single rear impact.

The energy applied to the seat was a factor in many of the cases. The energy transfer to the seat was estimated for each case and it was higher than 5,500 J in 15 of the 22 cases. This energy level is considered exceedingly severe, compromising the ride-down space available, even though the seats, head restraints, seat belts and vehicle structures performed well in crash-safety rating programs. As described by Horsch [56], design alternatives which lower the injury response in a specific impact severity are not necessarily the best design alternative at other severities. For example, James *et al.* [57] used Horsch's methodology to predict an overall increase in injuries if a side airbag was optimised to reduce 50% of injuries at delta Vs of 43 km/h or above. The authors reported that this optimisation would result in a 1% increase in injuries at a delta V of 21 km/h or below. Since most side-impact crashes occur at lower speeds, while few occur at delta V of 43+ km/h, James *et al*. [57] estimated a 12% overall increase of injuries. A similar analysis regarding increasing seat stiffness was conducted for rear impacts [18]. The results estimated an increase in the risk of serious-to-fatal injury by up to 6.9 times if stiffer ABTS seats replaced conventional seats in all passenger vehicles.

Ramping

Ramping was observed in some cases. Ramping has been defined as the displacement, 7.5 cm or greater, of the hip and lower back along the seat back [8]. Ramping may occur when the seat reaches its maximum yield and the seatback reaches its peak deflection, when the seat drops down from vehicle override and/or when the seatback is or becomes supported. Under these circumstances, the occupant can move up the seatback due to the longitudinal force and backrest angle, depending on friction and pocketing. Ramping has not been observed in rear tests up to 40 km/h with the 50th Hybrid III lap-shoulder belted in modern seats due to the retention designs. Ramping has however been observed at 49 km/h or greater [45].

Case 4 provides an example of ramping, which occurred when the seat back became supported by contact with the intruded child restraint seat in the 2nd row. Localised loading occurred due to the bolstering of the seat back as it became supported. The seat-back rotation was limited and resulted in changes in occupant kinematics. The occupant moved up and his head likely contacted the roof structures, resulting in “buckling” of the spine with localised compression-flexion in his cervical spine.

Extension Loading

The in-depth case review of the radiology records indicated that most thoracic spine injuries resulted from extension loading. This itself is interesting since extension injuries to the thoracic spine are relatively rare [58]. Vertebral body fracture code definitions in the AIS dictionary are primarily based on extent of compression and do not reflect the characteristics of extension-type injuries [43]. Therefore, AIS coding alone should not be used as a surrogate to imply fracture type or mechanism. Extension from the initial spine straightening along the seat back was most common – it was observed in 13 of the 24 spine areas with AIS2+ spine injuries. It should be noted that the head and shoulders can lift during the straightening of the curvature of the spine and may load the head restraints, as observed in some cases (Appendix E).

Extension from fulcrum loading was observed in only two of the 24 cases (cases 1 & 8). Fulcrum loading occurred when the head was misaligned with the head restraint due to oblique loading and was no longer supported. In both cases, the intrusion was severe and supported the seat. Injuries occurred in the cervical spine. Hyperextension was first discussed by Viano in 2011 [59]. It was associated with offset loading, when the thoracic spine hinged around the seat-back frame while the seat backs remained relatively upright. Some cases examined in [59] were later discussed in Viano *et al.* [6]. One case occupant had a history of DISH, and another had stenosis and spine degeneration, including ankylosis. The fractures in these pathologically stiffened spines likely occurred early during spine straightening, with the fulcrum loading exacerbating the injury and resulting in more severe retrolisthesis.

There was no radiology for one of the cases in [59], but the 61-year-old right-front passenger was exposed to a left-rear impact with override. In the crash, the occupant ramped up the backrest while moving inboard. His spine hinged on the inboard side of the upper seat-back frame. A case involving a 22-year-old obese female driver involved an override impact. There was severe intrusion that supported the driver’s seat back. She moved up due to override, rearward, and outboard. Her head moved outboard of the head restraint and her shoulders displaced up and over the top of the seat back, causing extension of the thoracic spine at T3-T4.

Various studies have been conducted to assess the effect of offset loading on the spine in rear impacts using the Hybrid III ATD [10][60]. The results showed that the upper body moved off the seat back and extended rearward around the seat-back frame while the pelvis was restrained by the seat and lap belt. The thoracic spine of the ATD is rigid, so a more humanlike spine would have demonstrated even more extension around the seat back. These out-of-position tests simulate real-world situations, including occupants initially leaning on the centre console or movement of the occupant in a crash that involves an oblique rear direction or yaw motion of the vehicle so that the upper torso moves off the seat back. Since ABTS seats are stiff with more seat-back structure, the likelihood of the head or upper body sliding off the seat back is greater than with a yielding seat.

Spine Degeneration

A key finding of this study is the association between spine degeneration and injury outcome. The radiology review showed that 20 out of the 22 occupants had spine degeneration as quantified in the radiology images shown in Appendix E. Rudd and Parenteau [26] reported that motor vehicle occupants with spinal degenerative diseases were at 16.2 times higher risk for serious spine injury. Yoganandan *et al.* [61] tested spines with and without spine degeneration and reported lower biomechanical tolerance with degeneration.

Most cases involved spine stiffening disease, such as DISH and/or degenerative spondylosis. In 16 of the 20 cases with available radiology information, there was osseous bridging of the spinal column, creating a relatively long mechanical lever arm. The nearly rigid thoracic spine is unable to respond to imparted loads by distributing deformations over multiple flexible spinal motion segments, as a normal spine would. Patients with stiff spines are prone to fracture, even as a result of minor trauma, such as falling from a standing or sitting position [27]. Okada *et al*. [62] reported that in a series of 42 DISH patients treated for spinal fracture, 73.8% resulted from trivial trauma, and 54.8% developed paralysis. In a study of human cadaveric thoracic spinal segments, Rapp van Roden *et al.* [29] found that when compared to non-DISH-affected spinal specimens, DISH-affected specimens were four times more likely to fracture for a given extension moment, and 16 times more likely to fracture for a given extension angle.

When a motor vehicle occupant with an ankylosing spinal disorder, such as DISH, AS, or DS, sustains the forces imparted in a rear-impact collision, the forward acceleration of the occupant by the seat back attempts to straighten the kyphotic curvature of the thoracic spine, as the head and upper torso move rearward relative to the vehicle interior. While a normally flexible thoracic spine would straighten by extending over multiple intervertebral joints along the full length of the thoracic spine to distribute loads broadly over the spine and seatback, an ankylosed, stiff, brittle spine is unable to extend and instead cracks with extension-type fracture-dislocations [6-7]. These extension injuries can occur without the occupant ramping up the seat back or moving off the support from the seat back and head restraint [6].

Hyperkyphosis was observed in five of the 15 cases with available measurements. For a seated passenger with accentuated thoracic spinal kyphosis, the head, shoulders, and upper torso are positioned farther forward of the seat backrest compared to a seated passenger with a normal degree of thoracic spinal kyphosis. In a rear impact, the lower back and hips are accelerated forward by the lower section of the seat back, and the head and upper torso lag behind. The rearward inertia of the initially lagging head and upper torso relative to the forward accelerating lower spine and hips produces large spinal extension moments and rearward shear forces, which are accentuated in subjects with hyperkyphotic spines [7]. Cases 3, 12, 13, and 15 illustrate how hyperkyphosis likely increased the relative velocity between the occupant and the seat back, increasing injury potential and severity.

Osteoporosis was observed in seven of 17 cases where measurement was possible. Low bone mineral density lowers the load threshold at which vertebral bodies fail under compressive, tensile, and shear forces, rendering affected occupants disproportionately vulnerable to fracture. Trabecular attenuation values below approximately 130 Hounsfield units on CT correlate with osteoporosis and increased fracture risk, and are of particular relevance in occupants with co-existing ankylosing spinal disorders, in whom poor trabecular bone quality compounds the biomechanical vulnerability imposed by spinal rigidity [50][63].

Stenosis was observed in six of 19 cases where measurement was possible. In individuals with spinal canal stenosis, the spinal cord is tightly positioned within a narrowed canal, in contrast to a normal-calibre canal in which the spinal cord is surrounded by abundant cerebrospinal fluid and cushioned by epidural fat. Smaller spinal canal diameter correlates significantly with spinal cord injury, while larger diameter confers relative protection [64-65]. In a study of 45 patients suffering from acute spinal cord injury and 68 patients showing no neurological symptoms after minor trauma to the cervical spine, Aebli *et al*. [52] found that narrow spinal canals predispose patients to spinal cord injury following minor trauma. Using a Torg ratio cutoff of 0.7 yielded a positive predictive value of 75% and a positive likelihood ratio of 51 for spinal cord injury following minor trauma.

Radiological Patterns of Injury Mechanisms

Characteristic radiological patterns were associated with the two predominant injury mechanisms identified in this study: injury from interaction with the second row or roof (ramping and/or intrusion), and injury from spinal straightening/extension during rear impact. The ramping/intrusion pattern is characterised by head injury – specifically scalp haematoma near the head vertex with or without intracranial bleeding – and by spinal injury at higher levels, including the cervical and upper thoracic spine, reflecting the spine's management of torso mass following head impact. Imaging hallmarks include vertebral body flattening and/or characteristic compressive bone marrow edema on MRI, both indicative of compressive loading [40][66].

The spinal straightening/extension pattern, by contrast, occurs preferentially in occupants with pre-existing spinal stiffening disorders, including DISH and degenerative spondylosis, and characteristically involves disruption of the anterior longitudinal ligament. Fractures in this pattern are typically distracted or retrolisthetic; and critically, neither compressive vertebral body flattening nor compressive marrow edema is present. Injury localises to the mid-to-lower thoracic spine, though it may occur at higher levels depending on the location and rostral extent of pre-existing ankylosis.

Several caveats bear emphasis. In unstable fractures, injury configuration may change between the moment of injury and the time of imaging – for example, as a result of patient manipulation by first responders – potentially obscuring the initial displacement pattern. High-energy impacts may generate additional mechanisms, including rebound off the seat back, intrusion of the second-row seat, or cargo loading, each capable of producing overlapping or atypical imaging findings. Similarly, multiple discrete collisions within a single event can introduce additional injury mechanisms that complicate pattern attribution. Case 21 illustrates this challenge: neither the injury characteristics nor the vehicle evidence supported a conclusive determination of injury mechanism.

Post-Crash Care

To improve post-crash care, first responders should consider that older occupants may sustain potentially unstable thoracic spine fractures even in moderate severity rear impacts. Although not possible to know at the scene of a crash whether an occupant has pre-existing spinal conditions, the general association with age warrants additional precautions be considered. Treatment of the injuries generally aligned with the AIS severity of the injuries – application of a brace for spine AIS2 injuries and surgical fusion for AIS3 or higher injuries.

Limitations

There are limitations to this study related to the data source and the nature of follow-on crash investigations. Although CIREN cases contain extensive medical details, the lower overall case count and selection process limit statistical analysis. Furthermore, given that case identification and initiation is performed at trauma centres, overall injury severity of the case subjects tends to be higher. This study does not include an examination of outcomes for occupants with spinal degeneration who did not sustain spinal injury. No comparisons in injury outcome were attempted between crashes of similar severity for occupants with and without certain conditions. The condition of the vehicles at the time of inspection may not represent their condition immediately after the crash, so there is limited confidence that the seat reflects only impact-induced damage.

V. Conclusions

This study assessed causal factors and characteristics of spine injuries in lap-shoulder-belted front-seat occupants in rear-impact CIREN crashes from the USA. Most of the injuries occurred in the thoracic spine. Based on the damage-based crash severity, most were very severe and many involved subsequent impacts. Estimated energy absorbed by the seat was considered excessive in nearly three-quarters of the cases. The detailed review of radiology highlighted an association between spine degeneration and injury outcome. Previous literature has shown that occupants with spine degeneration have higher risk of serious injury, and this study included mostly occupants with pre-existing spinal conditions. Although other mechanisms were identified, a distinct pattern of injuries to the thoracic spine from extension was common for case subjects with stiffened spines due to loading against the seat back early in the crash sequence.

VI. Disclaimer

This publication was written in the interest of information exchange. The opinions, findings, and conclusions expressed are those of the authors and not necessarily those of the Department of Transportation or the National Highway Traffic Safety Administration. The United States Government assumes no liability for its content or use thereof. If trade or manufacturers' names or products are mentioned, it is because they are considered essential to the object of the publication and should not be construed as an endorsement. The United States Government does not endorse products or manufacturers.

VII. References

[1] McElhaney, J. H., Nightingale, R. W., Winkelstein, W. A., Cahncey, V. A., Myers, B. S. (2010) Biomechanical Aspects of Cervical Trauma. In: Nahum, A. M., Melvin, J. W., (eds), *Accidental Injury, Biomechanics and Prevention Second Edition*, pp. 324–369. *Springer-Verlag*: New York.

[2] Parenteau, C. S. and Viano, D. C. (2014) Spinal Fracture-Dislocations and Spinal Cord Injuries in Motor Vehicle Crashes. *Traffic Injury Prevention*, **15**(7): pp. 694–700. doi:10.1080/15389588.2013.867434.

[3] Burney R. E., Maio, R. F., Maynard, F., Karunas, R. (1993) Incidence, characteristics, and outcome of spinal cord injury at trauma centers in North America. *Archives of Surgery*, **128**(5): pp. 596–599. doi:10.1001/archsurg.1993.01420170132021.

[4] Parenteau, C., Burnett, R., Davidson, R. (2025) Overview of Seat Design Changes and Performance. SAE Technical Paper 2025-01-8729, Society of Automotive Engineers.

[5] Viano, D. C. and Parenteau, C. S. (2015) Update on the effectiveness of high retention seats in preventing fatal injury in rear impacts. *Traffic Injury Prevention*, **16**(2): pp. 154–158.

[6] Viano, D., Parenteau, C., White, S. (2019) Influence of DISH, Ankylosis, Spondylosis and Osteophytes on Serious-to-Fatal Spinal Fractures and Cord Injury in Rear Impacts. SAE Technical Paper 2019-01-1028, https://doi.org/10.4271/2019-01-1028.

[7] Davis, M., Isaacs, J., Graber, M., Fisher, J. (2019) Thoracic Spine Extension Injuries in Occupants with Pre-Existing Conditions during Rear-End Collisions. SAE 2019-01-1222, Society of Automotive Engineers.

[8] Viano, D., Burnett, R., White, S., Stephens, G., Parenteau, C. (2021) Dual-recliner ABTS Seats in Severe Rear Sled Tests with the 5th, 50th and 95th Hybrid III. SAE 2021-01-0917, Society of Automotive Engineers.

[9] Parenteau, C. S., Croteau, J., Zolock, J. (2020) The Effect of Crash Severity and Structural Intrusion on ATD Responses in Rear-End Crashes. SAE 2020-01-1224, Society of Automotive Engineers.

[10] Viano, D. C., Parenteau, C. S., Burnett, R., James, M. (2009) Influence of Seating Position on Dummy Responses with ABTS Seats in Severe Rear Impacts. SAE 2009-01-0250, Society of Automotive Engineers.

[11] Kang, Y. S., Stammen, J., Ramachandra, R., *et al.* (2020) Biomechanical Responses and Injury Assessment of Post-Mortem Human Subjects in Various Rear-facing Seating Configurations. *Stapp Car Crash Journal*, **64**(November 2020): pp. 155–212.

[12] Hagedorn, A. (2018) Rear-Facing Reclined Testing Sled Buck Design & ATD Tests. Automated Vehicle Occupant Safety Workshop, November 27.

[13] Parenteau, C. S. and Viano, D. C. (2021) Serious Head, Neck and Spine Injuries in Rear Impacts: Frequency and Sources. *Proceedings of the IRCOBI Conference*, 2021, Beijing, China, IRC-21-10.

[14] Burnett, R., Carter, J., Roberts, V., Myers, B. (2004) The influence of seatback characteristics on cervical injury risk in severe rear impacts. *Accident Analysis & Prevention*, **36**(4).

[15] Viano, D. C. and Parenteau, C. S. (2022) Injury by Delta V in Front, Near-Side, Far-Side and Rear Impacts: Analysis of 1994-2015 NASS-CDS. 2022-01-0835, Society of Automotive Engineers.

[16] Parenteau, C. S. and Burnett, R. (2025) Occupant Responses in High-Speed Rear Sled Tests: Focus of Initial Position, Seat Strength and ATD Size. SAE Technical Paper 2025-01-8731, Society of Automotive Engineers.

[17] Parenteau, C. S., White, S., Burnett, R., Stephens, G., Michalski, D. (2022) Rear-End Impacts – Part 1: Field and Test Data Analysis of Crash Characteristics. SAE 2022-01-0859, Society of Automotive Engineers.

[18] Parenteau, C. S., Viano, D. C., Burnett, R., Lau, E. (2021) Effect of ABTS and Conventional Seats on Occupant Injury in Rear Impacts: Analysis of Field and Test Data. *Traffic Injury Prevention,* **22**(7): pp. 553-558.

[19] Viano, D. C. and Parenteau, C. S. (2008) Serious Injury in Very-Low and Very-High Speed Rear Impacts. SAE 2008-01-1485, Society of Automotive Engineers.

[20] Lockerby, J. and Rudd, R. (2026) Rear-impact crash injury patterns and predictors: Insights from contemporary CISS and CIREN field data. *SAE Int. J. Trans. Safety*, **44**(1).

[21] Parenteau, C. S., Prasad, P., Burnett, R. (2008) Occupant responses in high-speed rear crashes: analysis of government-sponsored tests. SAE 2008-01-0188, Society of Automotive Engineers.

[22] Parenteau, C. S., Burnett, R., Viano, D. C., White, S. (2021) Effect of Occupant Weight and Initial Position in Low-to-High Speed Rear Sled Tests with Older and Modern Seats. SAE 2021-01-0918, Society of Automotive Engineers.

[23] Edwards, M., Viano, D. C., Parenteau, C. S. (2009) Analysis of Front-Seat Occupant Injuries in Rear Impacts. SAE 2009- 01-1200, Society of Automotive Engineers.

[24] Galli, R. M. and Digges, K. (2008) Severe Head and Neck Injuries in NASS Rear Impacts. SAE 2008-01-0190, Society of Automotive Engineers.

[25] Viano, D. C. and Parenteau, C. S. (2018) Severe Injury in Multiple Impacts: Analysis of 1997-2015 NASS-CDS. *Traffic Injury Prevention*, **19**: pp. 1–17.

[26] Rudd, R. W. and Parenteau, C. S. (2023) Serious Spine Injuries Using 2017-2021 CISS and CIREN Data: Effect of Spinal Degeneration Comorbidities. *Proceedings of the IRCOBI Conference*, 2023, Cambridge UK.

[27] Shah, N. G., Keraliya, A., *et al*. (2019) Injuries to the Rigid Spine: What the Spine Surgeon Wants to Know. *Radiographics*, **39**(2): pp. 449–466.

[28] Westerveld, L. A., Verlaan, J. J., Oner, F. C. (2009) Spinal fractures in patients with ankylosing spinal disorders: a systematic review of the literature on treatment, neurological status and complications. *European Spine Journal*, **18**(2): pp. 145–156.

[29] Rapp van Roden, E. A., Riggin, C. N., *et al*. (2025) Influence of Spinal Bridging Ossification on Mechanical Properties and Fracture Tolerance Under Flexion/Extension Loading. *Annals of Biomedical Engineering*, **53**(10): pp. 2679–2688.

[30] Kuperus, J.S., Samsour, L., *et al.* (2018) Bone mineral density changes over time in diffuse idiopathic skeletal hyperostosis of the thoracic spine. *Bone*, **112**: pp. 90-96.

[31] Diederichs, G., *et al.* (2011) Osteoporotic Fractures in Men Research Group. Diffuse idiopathic skeletal hyperostosis (DISH): relation to vertebral fractures and bone density. Osteoporosis International, **22**(6): pp. 1789-1797.

[32] Takao, T., *et al*. (2013) Clinical relationship between cervical spinal canal stenosis and traumatic cervical spinal cord injury without major fracture or dislocation. *European Spine Journal*, **22**(10): pp. 2228–2231.

[33] Brinjikji, W., *et al*. (2015) Systematic literature review of imaging features of spinal degeneration in asymptomatic populations. AJNR *American Journal of Neuroradiology*, **36**(4): pp. 811–816.

[34] Theodore, N. (2020) Degenerative cervical spondylosis. NEJM, **383**: pp. 159–168.

[35] Nachemson, A., Schultz, A. B., Berkson, M. H. (1979) Mechanical properties of human lumbar spine motion segments: Influences of age, sex, disc level, and degeneration. *Spine*, **4**(1): pp. 1–8.

[36] Greaves, L. L., *et al*. (2009) Pediatric and adult three-dimensional cervical spine kinematics: Effect of age and sex through overall motion. *Spine*, **34**(16): pp. 1650–1657.

[37] Benoist, M. (2003) Natural history of the aging spine. *European Spine Journal*, **12**(S2): pp. S86–S89.

[38] Kaushal, M., *et al*. (2014) MDCT of acute subaxial cervical spine trauma: a mechanism-based approach. *Insights into Imaging*, **5**(3): pp. 321–338.

[39] Miele, V., Trinci, M., Galluzzo, M., *et al*. (2022) Cervical spine injury: clinical and medico-legal overview. *La Radiologia Medica*, **127**(10): pp. 1047–1061.

[40] Kumar, Y. and Hayashi, D. (2016) Role of magnetic resonance imaging in acute spinal trauma: a pictorial review. *BMC Musculoskeletal Disorders*, **17**(310).

[41] National Highway Traffic Safety Administration. "Crash Injury Research". Internet: https://www.nhtsa.gov/research-data/crash-injury-research. [2026 March 01].

[42] Schneider, L., Rupp, J., *et al.* (2011) BioTab – A New Method for Analyzing and Documenting Injury Causation in Motor Vehicle Crashes. *Traffic Injury Prevention*, **12**: pp. 256–265.

[43] The Abbreviated Injury Scale 2015 Revision (2016) AAAM. Des Plaines, IL, USA.

[44] Yaek, J., Brown, T., Goertz, A. (2020) Accident Statistical Distributions from NASS CDS - An Update. SAE Technical Paper 2020-01-0518.

[45] Parenteau, C. S., Burnett, R., Davidson, R. (2026) Occupant and Seat Responses in Various Rear Impact Conditions: Focus on Head-to-Head Restraint Interactions. SAE Technical Paper 2026-01-0565.

[46] Resnick, D. and Niwayama, G. (1976) Radiographic and pathologic features of spinal involvement in diffuse idiopathic skeletal hyperostosis (DISH). *Radiology*, **119**(3): pp. 559–568.

[47] Diekhoff, T., *et al*. (2022) MRI in axial spondyloarthritis: understanding an 'ASAS-positive MRI' and the ASAS classification criteria. *Skeletal Radiology*, **51**(9): pp. 1721–1730.

[48] Park, M. S., Lee, Y. B., *et al*. (2014) Facet joint degeneration of the cervical spine: a computed tomographic analysis of 320 patients. *Spine*, **39**(12): pp. E713–E718.

[49] Liebsch, C., Greiner-Perth, A. K., *et al.* (2025) Intervertebral disc degeneration, age, and sex affect the range of motion of the cervical spine. Scientific Reports, **15**: 23540.

[50] Liebsch, C., Tao, Y., *et al*. (2022) Validity and interobserver agreement of a new radiographic grading system for intervertebral disc degeneration: Part III. Thoracic spine. *European Spine Journal*, **31**: pp. 726–734.

[51] Castillo-López, J. A., Bravo-Ontiveros, F., Rodea-Montero, E. R. (2023) Identification of Bone Mineral Density Deficit Using L1 Trabecular Attenuation by Opportunistic Multidetector CT Scan in Adult Patients. *Tomography*, **9**(1): pp. 150–161.

[52] Aebli, N., Wicki, A. G., *et al*. (2013) The Torg-Pavlov ratio for the prediction of acute spinal cord injury after a minor trauma to the cervical spine. *Spine Journal*, **13**(6): pp. 605–612.

[53] Scoles, P. V., Linton, A. E., Latimer, B., Levy, M. E., Digiovanni, B. F. (1988) Vertebral body and posterior element morphology: the normal spine in middle life. *Spine*, **13**(10): pp. 1082–1086.

[54] Fon, G. T., Pitt, M. J., Thies, A. C. (1980) Thoracic kyphosis: range in normal subjects. *American Journal of Roentgenology*, **134**(5): pp. 979–983.

[55] Digges, K. and Bahouth, G. (2003) Frequency of Injuries in Multiple Impact Crashes. *Association for the Advancement of Automotive Medicine*, **47**: pp. 417–423.

[56] Horsch, J. (1987) Evaluation of Occupant Protection from Responses Measured In Laboratory Tests. SAE Technical Paper 870222.

[57] James, M., Strother, C., *et al.* (1991) Occupant Protection in Rear-end Collisions: I. Safety Priorities and Seat Belt Effectiveness. SAE Technical Paper 912913.

[58] Denis, F. and Burkus, J. K. (1992) Shear fracture-dislocations of the thoracic and lumbar spine associated with forceful hyperextension (lumberjack paraplegia). *Spine*, **17**(2): pp. 156–161.

[59] Viano, D. C. (2011) Fracture-dislocation of the thoracic spine in extension with upright seats in severe rear crashes. Society of Automotive Engineers. SAE 2011-01-0274.

[60] Burnett, R. A., Parenteau, C. S., White, S. D. (2023) The effect of seatback deformation on out-of-position front-seat occupants in severe rear impacts. *Traffic Injury Prevention*, **24**(3): pp. 184–188.

[61] Yoganandan, N., Ray, G., Pintar, F. A., Myklebust, J., Sances, A. (1989) Stiffness and strain energy criteria to evaluate the threshold of injury to an intervertebral joint. *Journal of Biomechanics*, **22**: pp. 135–142.

[62] Okada, E., Tsuji, T., *et al*. (2017) CT-based morphological analysis of spinal fractures in patients with diffuse idiopathic skeletal hyperostosis. *Journal of Orthopaedic Science*, **22**(1): pp. 3–9.

[63] Schreiber, J. J., Anderson, P. A., Rosas, H. G., Buchholz, A. L., Au, A. G. (2011) Hounsfield units for assessing bone mineral density and strength: a tool for osteoporosis management. *The Journal of Bone and Joint Surgery – American Volume*, **93**(11): pp. 1057–1063.

[64] Matsuura, P., Waters, R. L., *et al*. (1989) Comparison of computerized tomography parameters of the cervical spine in normal control subjects and spinal cord-injured patients. *The Journal of Bone and Joint Surgery – American Volume*, **71**(2): pp. 183–188.

[65] Eismont, F. J., Clifford, S., Goldberg, M., Green, B. (1984) Cervical sagittal spinal canal size in spine injury. *Spine*, **9**(7): pp. 663–666.

[66] Brinckman, M. A., Chau, C., Ross, J. S. (2015) Marrow edema variability in acute spine fractures. *Spine Journal*, **15**(3): pp. 454–460.

VIII. APPENDIX

Appendix A

TABLE AI

VEHICLE AND CRASH DETAILS

Crash #	Occ. #	CIRENID	Model Year	Make	Model	# Ev.	Sequential CDCs w/ rank	Rank 1 PDOF	Rank 1 Delta V (km/h)	Exc. Sev. *	Oblique **	Mult. Event
1	1	86	2012	Nissan	Maxima	1	1: 05BZAW07	160	98	Y	Y	
2	2	141	2015	Chevrolet	Spark	1	1: 06BDEW03	180	41			
3	3	298	2016	Honda	HR-V	3	1: 06BDEW02 2: 12FREW02 3: 12FLES02	170	34			Y
4	4	441	2015	Hyundai	Santa Fe	1	1: 06BDAW04	170	145	Y		
5	5	665	2015	Chevrolet	Equinox	1	1: 06BZEW04	170	37			
6	6	681	2018	Honda	CR-V	2	1: 06BZAW03 2: 12FREE04	170	65	Y		Y
7	7	704	2017	GMC	Yukon XL	1	1: 06BYEW03	180	49			
8	8	709	2009	Toyota	Camry	2	1: 07BLEW08 2: 11FYEW02	200	95	Y	Y	Y
9	9	804	2014	Toyota	Prius	3	1: 06BDEW03 2: 01FZEW01 3: 12FLEE01	190	70	Y		Y
9	10	805	2014	Toyota	Prius	3	1: 06BDEW03 2: 01FZEW01 3: 12FLEE01	190	70	Y		Y
10	11	1070	2017	BMW	X3	1	1: 06BDAW04	180	56	Y		
11	12	1101	2018	Mercedes-Benz	GLS	1	1: 06BDEW02	180	30			
12	13	980018	2023	GMC	Sierra	2	1: 06BYEW01 2: 00UZLW02	190	34			Y
13	14	980021	2017	Infiniti	Q50	2	1: 06BYEW08 2: 99U99999	190	79	Y		Y
14	15	980038	2018	Subaru	XV	1	1: 06BDEW04	170	54			
15	16	980076	2015	Chevrolet	Malibu	2	1: 06BREE06 2: 09LPEW01	170	76	Y		Y
16	17	980090	2014	Chevrolet	Impala	2	1: 06BDEW06 2:06B9MW01	180	71	Y		Y
16	18	980091	2014	Chevrolet	Impala	2	1: 06BDEW06 2:06B9MW01	180	71	Y		Y
17	19	980114	2024	Chevrolet	Blazer	2	1: 06BYEW02 2: 02RPEW01	180	30			Y
18	20	980121	2024	Toyota	RAV4	2	1: 06BYEW03 2: 11LDES01	190	53			Y
19	21	980150	2015	Audi	A3	2	1: 06BDEW06 2: 12FDEW02	180	41			Y
20	22	980340	2014	Lexus	IS-250	3	1: 06BDAW06 2: 12FDEW02 3: 01FYEW01	180	BES: 80			Y

Appendix B

TABLE BI

OCCUPANT DETAILS AND FACTORS

	Seat		Other Factors

Crash #	Occ. #	Seat	Condition	Head Rest.	Age	Sex	Height (cm)	Weight (kg)	BMI	MAIS	Age	Obese	Other	Seat Energy
1	1	D	Intrusion supp	Loaded & support	25	M	175	123	40.2	6		Y		Y
2	2	D	Cargo supp	Loaded	41	F	157	117	47.5	5		Y		
3	3	D	Occ load.	Loaded	65	M	178	128	40.4	4		Y		
4	4	D	Cargo supp	Loaded & removed	67	M	163	63	23.7	3				Y
5	5	D	Occ load.	Loaded	80	F	182	113	34.1	3	Y	Y		
6	6	D	Occ load.	Loaded	74	M	178	102	32.2	3	Y	Y		Y
7	7	D	No def.	Loaded	74	M	180	140	43.2	3	Y	Y		Y
8	8	D	Intrusion	Loaded & support	59	F	157	85	34.5	4		Y		Y
9	9	D	Occ load.	Loaded & removed	60	M	191	95	26.0	3			Belt mis-routing	Y
	10	RF	Occ load.	Loaded	57	F	168	68	24.1	4				Y
10	11	RF	Occ load.	Loaded	78	M	175	109	35.6	3	Y	Y		Y
11	12	D	Occ load.		73	M	170	123	42.6	3	Y	Y		
12	13	D	Occ load. Twisted outboard		72	M	180	98	30.2	3	Y	Y		Y
13	14	D	Occ load. & intrusion supp		51	M	193	102	27.4	4				Y
14	15	D	Occ load.	Loaded	53	M	185	93	27.2	2				Y
15	16	RF	Occ load & seat-track anchors separation		42	F	180	112	34.6	5		Y		Y
16	17	D	Occ load. (riser detach)	Removed	73	M	175	95	31.0	4	Y	Y		Y
	18	RF	Occ load.	Removed	72	F	163	94	35.4	3	Y	Y		Y
17	19	D	Occ load.	Damaged	62	F	160	79	30.9	3		Y		
18	20	D	No def		40	M	175	113	36.9	3		Y		Y
19	21	D	Occ load.		60	F	170	71	24.6	4				
20	22	D	Occ load.		69	F	165	73	26.8	5				Y
				ave.	61.2		173.6	99.8	33.1	3.6				
				sd	11.8		10.1	20.1	6.5	0.8				

Appendix C

TABLE CI

INJURY DETAILS AND CAUSAL FACTORS

#	Occ #	MAIS	AIS 2+ Spine (AIS)			# AIS 2+	Rib fx.	Mechanism	Factors			Treatme
			Cervical	Thoracic	Lumbar				Spine deg	Fusion	Other	
1	1	6	A-O disl (3) C1 fx (2) Odontoid fx (3)			3	Y	Tension w/ some extension				None - fata
2	2	5		T5-T6 fx/dislo. (5)		1	Y	Extension w/ subsequent flexion	Y		Object suppot	Fusion T4
3	3	4		T8-T9 distraction VB (3)		1	Y	Extension	Y			Fusion T8
4	4	3	C7 bil lamina fx (2) C7 TP fx (2)			1		Compression-flexion (buckling)	Y		Object support	Cervical c
5	5	3		T2 fx (2) VB minor compression		1	Y	Extension	Y			None documen
6	6	3		T10 burst fx (3)		1		Extension	Y			TLSO Bra
7	7	3		T5 fx disl w/ transient neuro signs (3)	L1 mamillary process fx (2)	2		Extension	Y			Fusion T2
8	8	4	C2 fx/disl. (4)			1	Y	Tension w/ some extension	Y		Intrusion support	Fusion C1
9	9	3		T9 minor VB fx/disl. (2) T10 minor VB fx/disl. (2)		2	Y	Flexion-distraction w/ anterior spinal column compression	Y		Torso belt under arm	CTO Bra
	10	4	C7 minor VB comp fx (2)	T1 minor VB comp fx (2)		2	Y	Compression-flexion (buckling)				TLSO Bra
10	11	3		T3 minor VB fx (2) T9 bilat facet fx (3) T10 bilat facet (3) and minor VB (2) fx and disc herniation (2)		4		Extension (T10) (1st) Compression w/flexion (T3)	Y			Fusion T8
11	12	3		T10 VB and posterior element fx (3)		1		Extension	Y			TLSO Bra
12	13	3		T6 VB and posterior element fx (3)		1	Y	Extension	Y	Y		Fusion T3
13	14	4		T3 VB minor compression fx (2)		1	Y	Compression-flexion (buckling)				None documen
14	15	2		T4 bilateral pedicle and VB fx (2)		1		Extension	Y			CTO Bra
15	16	5	C5 fx/disl complete cord (5) C6 TP/ lam/fac fx (2) C7 minor VB fx (2)			3	Y	Compression-flexion (buckling)	Y			Fusion C3
16	17	4			L2 disc rupt (3)	1		Extension	Y	Y		Fusion T12
	18	3		T6 minor VB fx (2) T7 minor VB fx (2)		2	Y	Extension	Y			None documen
17	19	3		T6 minor VB fx (2) T7 major burst VB fx (3) T8 bilateral pedicle fx (2)	L1 VBFX(2)	4		Extension	Y			CTLSO Br
18	20	3	C7 major VB fx (3)	T1 minor VB fx (2) T11 major VB fx (3) T10 disc (2)		4	Y	Extension (T10) (1st) Compression w/flexion (C7-T1)	Y			Fusion T4
19	21	4		T10 fx/disl incomplete cord fx (4)		1	Y	Unclear, likely flexion	Y			Fusion T8-T
20	22	5		T12 fx w/ incomplete cord (4) T11 TP &SP &minor VB fx (2)		2	Y	Compression &flexion	Y		Intrusion	Fusion T1

Appendix D

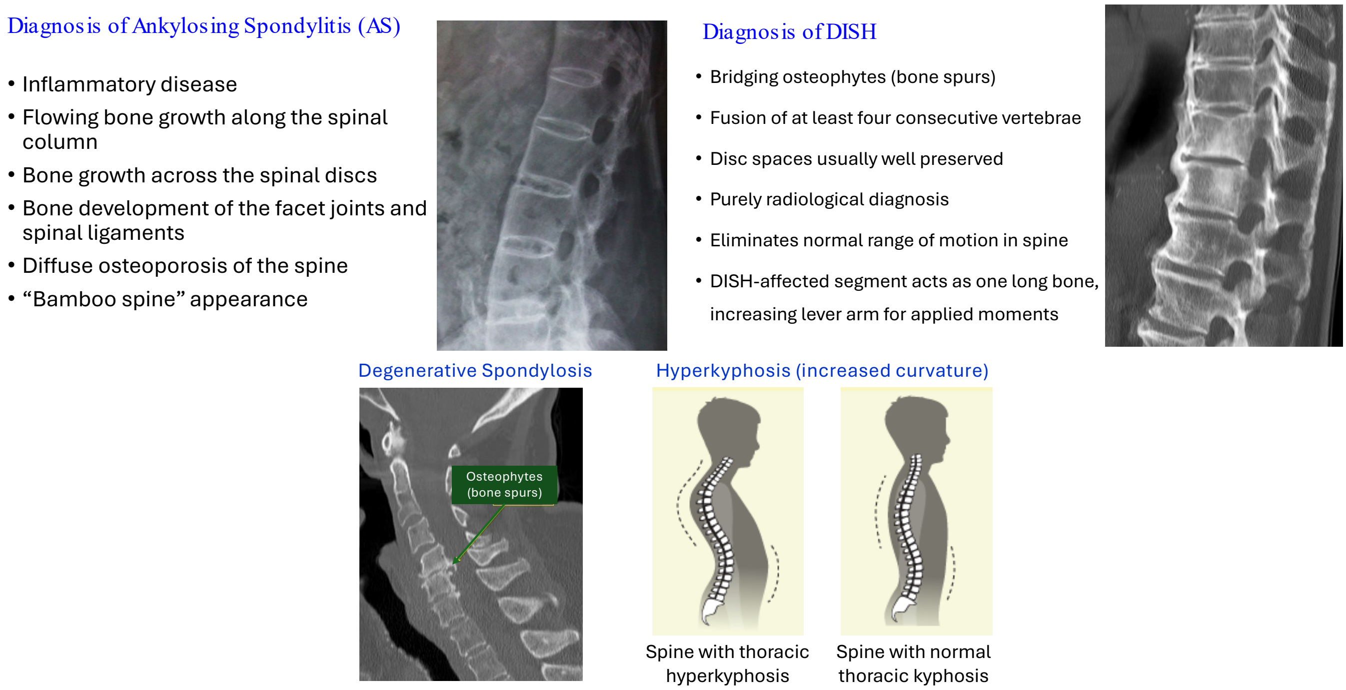

Fig. D1. Definitions of degenerative spine conditions.

TABLE DI
SUMMARY OF SPINAL DEGENERATION FINDINGS FOR CASE OCCUPANTS

Case #	CIREN ID	Osteoporosis	Canal Stenosis	Hyperkyphosis	DISH/DegenSpond (DS)	NOTES
1	86					No relavant imaging
2	141	NO	NO	NO	DISH+DS	
3	298	NO	YES	YES	DS	
4	441		YES	NO	DS	No CT to measure L1 HU
5	665	YES	NO	NO	DISH+DS	
6	681	NO	NO	NO	DISH+DS	
7	704				DISH+DS	Insufficient imaging
8	709		NO	N/A	DS	No CT to measure L1 HU
9	804	YES	NO	NO	DS	
10	805	NO	NO	N/A	NO	
11	1070	YES	YES	NO	DISH	
12	1101	NO	NO	YES	DISH+DS	
13	980018	YES	YES	YES	DISH+DS	
14	980021	NO	NO	NO	NO	
15	980038	NO	NO	YES	DISH	
16	980076	NO	NO	N/A	NO	
17	980090	YES	YES	N/A	DISH+DS	
18	980091			YES	DISH	Insufficient imaging
19	980114	YES	NO	NO	DISH+DS	
20	980121	YES	NO	NO	DISH+DS	
21	980150	NO	YES	NO	NO	
22	980340	NO	NO	NO	DISH+DS	

Appendix E

Case 1
CIREN ID 86

2012 Nissan Maxima
Object: brick column
Delta V: 98 km/h
PDOF: 160 deg
CDC: 05BZAW07
Seat energy: 29,623 J
Factors
Oblique loading
Crash severity
2nd row intrusion supporting seat

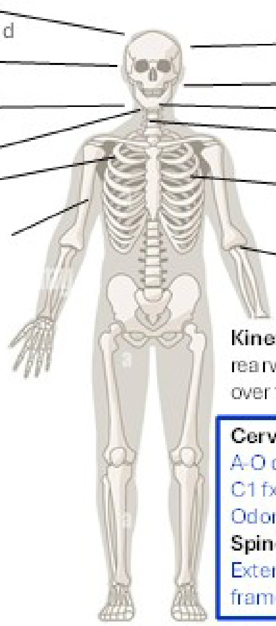

Driver
25yo Male (MAIS 6, fatal)
175 cm, 123 kg
Factor
Morbid obesity (BMI: 40.2)

Kinematics: During the 5 o'clock impact, the occupant moved rearward and inboard. The head and neck complex extended over the supported seatback, inboard of the head restraint.

Cervical Injuries
A-O disl (AIS 3)
C1 fx (AIS 2)
Odontoid fx (AIS 3)
Spine injury mechanism:
Extension from fulcrum loading on inboard upper seatback frame due to offset loading

Note: only X-rays were taken at the time of the autopsy.

Case 2
CIREN ID 141

2015 Chevrolet Spark
Striking: Large pickup
Delta V: 41 km/h
PDOF: 180 deg
CDC: 06BDEW03
Seat energy: 4,932 J

Factors
2nd row cargo supporting seatback

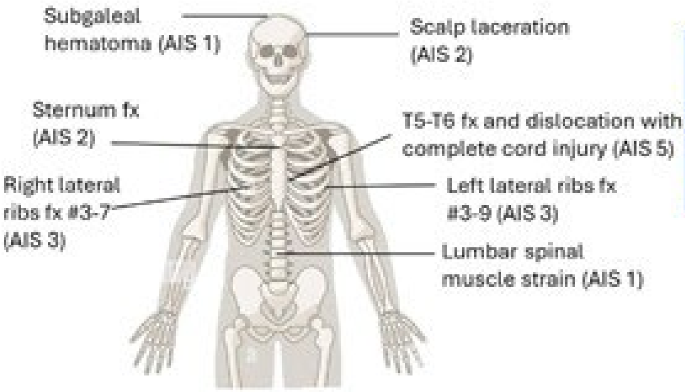

Thoracic spine injury
T5-T6 fx/dislocation (AIS 5)
Spine injury mechanism:
Extension from spine straightening, follwed by flexion loading during rebound.

Driver
41yo Female (MAIS 5)
157 cm, 117 kg
Factors
Morbid obesity (BMI: 47.5)
Pre-existing stiffening of spine (DISH & DS)

Kinematics: The occupant moved rearward with the PDOF and loaded the seat. The occupant pocketed into the seatback. The fused thoracic spine straightened along seatback and fractured. The seatback rotation was stopped by backseat cargo (boxes of paper). Her body likely ramped as she rebounded forward. The head loaded the underside of the head restraint.

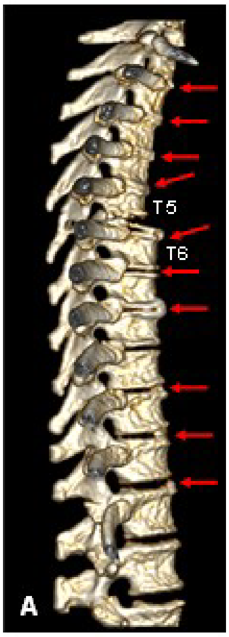

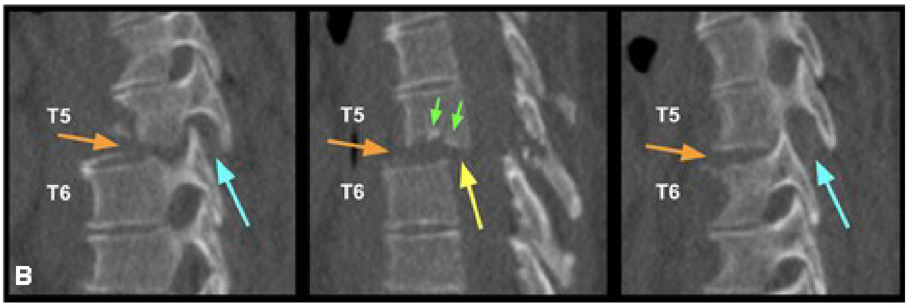

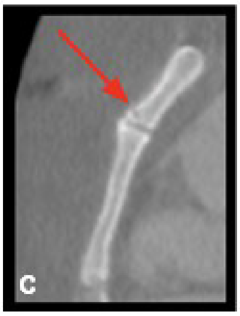

CASE 2. (A) Right lateral view of 3D reconstruction of thoracic spine demonstrates multilevel degenerative spondylosis and early DISH, stiffening the spine, with narrowing and osteophytic bridging of the anterior aspects of the disc spaces (red arrows). (B) Sagittal CT images demonstrate extension fracture-subluxation at T5-T6, with disruption of the anterior longitudinal ligament and widening/distraction of the anterior aspect of the disc space (orange arrows), retrolisthesis of T5 on T6 (yellow arrows), widening of the bilateral facet joints (blue arrows), and compressive flattening of the T5 vertebral body (green arrows). (C) Sagittal CT image demonstrates nondisplaced fracture of the sternal manubrium (red arrow).

Case 3

CIREN ID 298

2016 Honda HR-V
Striking: Passenger car
Delta V: 34 km/h
PDOF: 170 deg
CDC: 06BDEW02
Seat energy: 3,711 J
Factors
Oblique rear
Multiple impacts:

- Front w/ large PU (CDC: 12FLES02)
- Front w/ guardrail (CDC: 12FREW02)

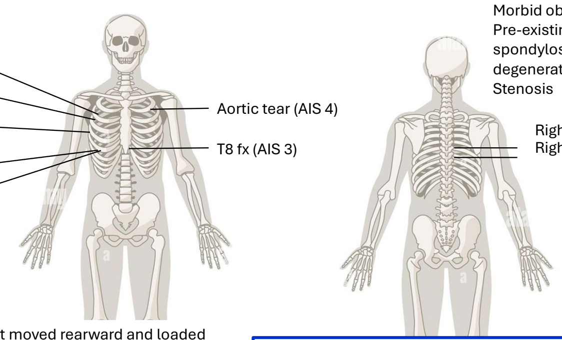

Factors
Morbid obesity (BMI: 40.4)
Pre-existing stiffening of spine due to spondylosis & DISH-like degeneration. Hyperkyphosis & Stenosis

Driver
65 yo Male (MAIS 4)
178 cm, 128 kg

Kinematics: The occupant moved rearward and loaded the seat. He pocketed into the seatback and straightened his stiffened spine along the seatback as it rotated. The seat yielded to maximum deflection for applied energy and the occupant rebounded forward. He also moved forward during the secondary frontal impacts.

Thoracic spine injury
Right T8 vertebrae (AIS 3)
Spine injury mechanism:
Extension due to forced straightening of fused spine

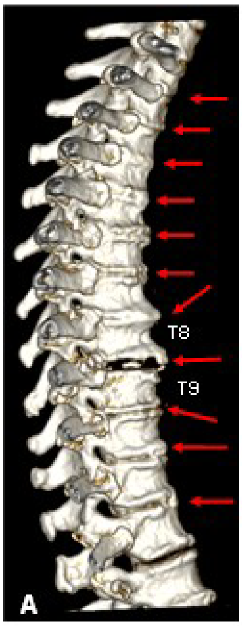

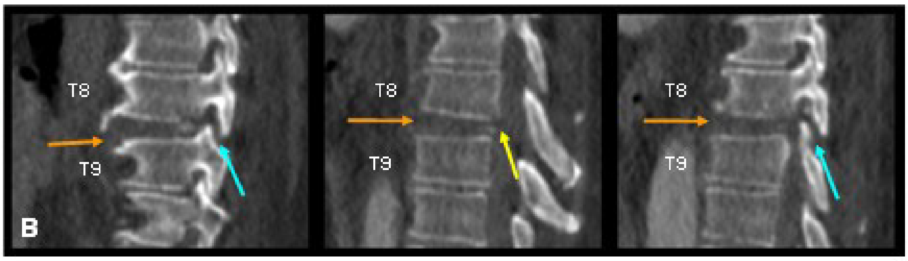

CASE 3. (A) Right lateral view of 3D reconstruction of thoracic spine demonstrates multilevel degenerative spondylosis, stiffening the spine, with narrowing and osteophytic bridging of the anterior aspects of the disc spaces (red arrows). (B) Sagittal CT images demonstrate extension fracture-subluxation at T7-T8, with disruption of the anterior longitudinal ligament and widening/distraction of the anterior aspect of the disc space (orange arrows), minimal retrolisthesis of T8 on T9 (yellow arrow), widening of the bilateral facet joints (blue arrows). No compressive vertebral body flattening is observed.

Case 4
CIREN ID 441

2015 Hyundai Santa Fe
Striking: Large PU
Delta V: 145 km/h
PDOF: 170 deg
CDC: 06BDAW04
Seat energy: 33,217 J

Factors
Crash severity
Cargo contact

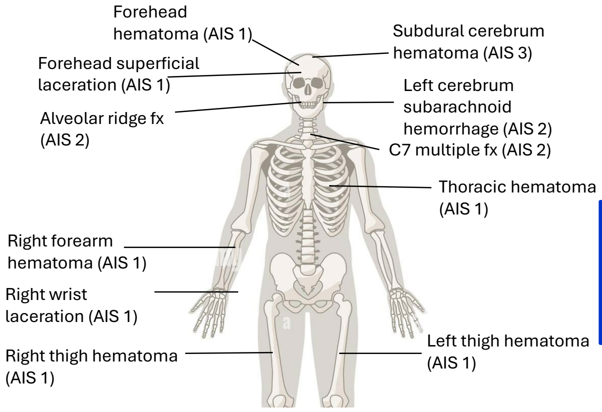

Driver
67yo Male (MAIS 3)
163 cm, 63 kg
Factors
Severe intrusion
Spine stiffnening due to degenerative spondylosis
Stenosis

Cervical spine injury
Bilateral lamina vertebrae C7 fx. (AIS 2)
Spinous process vertebrae C7 fx. (AIS 2)
Spine injury mechanism:
Axial compression resulting in localized buckling in flexion

Kinematics: The crash was severe. The crush and intrusion likely occurred early, pushing the 2nd row seat forward. There was a child seat in the left-rear. The case occupant moved rearward and inboard, loading the seat and head restraint. The seatback likely contacted the CRS that was pushed forward with intrusion, bolstering the seat. The occupant likely ramped up the seatback. The head may have contacted the roof structures. The head restraint showed signs of loading and was pulled out of its mounting. The occupant then rebounded forward.

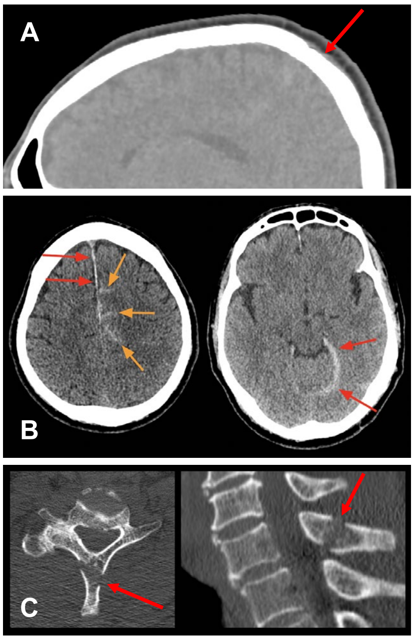

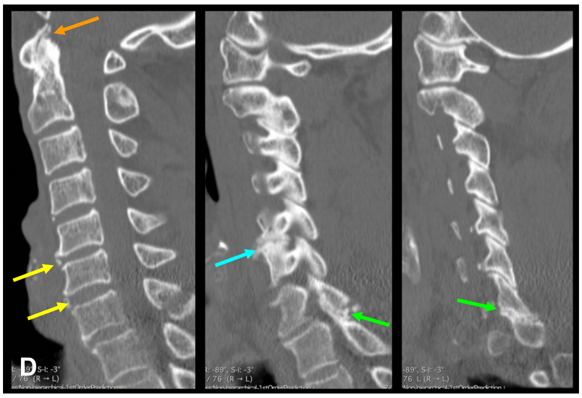

CASE 4. (A) Sagittal CT image demonstrates small scalp hematoma posterior to head vertex (red arrow). **(B)** Axial CT images demonstrate intracranial subdural (red arrows) and subarachnoid blood (orange arrows). **(C)** Axial (left) and sagittal (right) CT images demonstrate fracture of the C7 spinous process (red arrows), consistent with compression-flexion loading following spinal buckling. **(D)** Sagittal CT images demonstrate cervical degenerative spondylosis with osteophytic narrowing of the atlantodental joint (orange arrow), calcified anterior longitudinal ligament (yellow arrows), disc space narrowing/osteophytosis (blue arrow), and facet joint narrowing/osteophytosis (green arrows).

Case 5
CIREN ID 665

2015 Chevy Equinox
Striking: SUV
Delta V: 37 km/h
PDOF: 170 deg
CDC: 06BZEW04
Seat energy: 3,879 J

Factors
Oblique loading

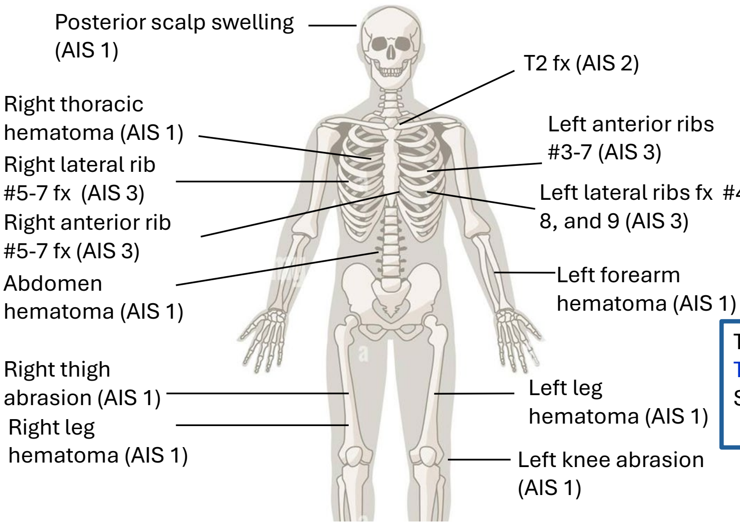

Driver
80yo Female (MAIS 3)
182 cm, 113 kg

Factors
Obesity (BMI: 34.1)
Age
Spine stiffening above & below injury location. DISH, degenerative spondylosis & osteoporosis

Thoracic spine injury
T2 vertebrae fx (AIS 2)
Spine injury mechanism:
Extension due to forced straightening

Kinematics: The driver moved rearward and loaded the seat. She pocketed into the seatback and straightened her stiffened spine along the seatback as it rotated. The driver moved slightly inboard with PDOF. The seat yielded. The seatback contacted the second -row seat cushion The driver likely ramped. The head restraint showed signs of occupant loading.

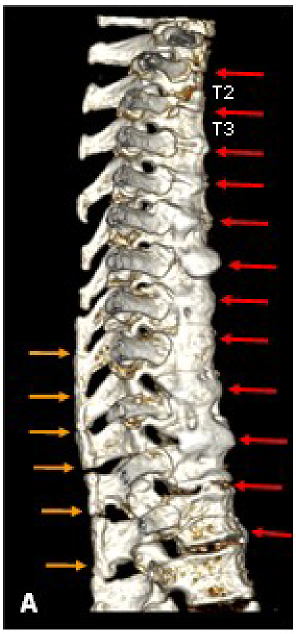

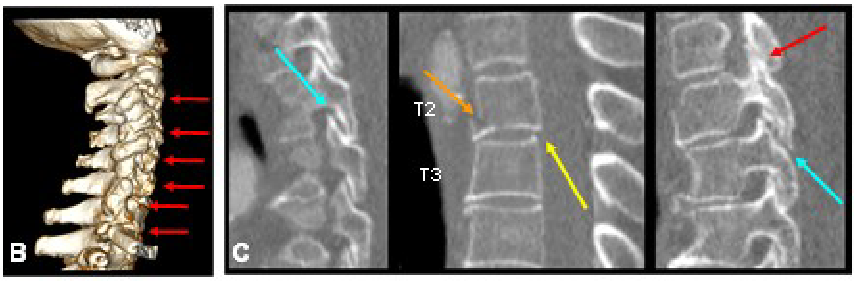

CASE 5. (A) Right lateral view of 3D reconstruction of thoracic spine demonstrates multilevel degenerative spondylosis and DISH, stiffening the spine, with narrowing and osteophytic bridging of the anterior aspects of the disc spaces (red arrows). Multilevel ossification of the supraspinous ligament (orange arrows) further stiffens the spine. (B) Right lateral view of 3D reconstruction of cervical and upper thoracic spine demonstrates multilevel degenerative spondylosis, stiffening the spine, with narrowing and osteophytic bridging of the anterior aspects of the disc spaces (red arrows). (C) Sagittal CT images demonstrate extension fracture-subluxation at T2-T3, with disruption of the anterior longitudinal ligament and mild distraction of fracture fragments at the anteroinferior margin of the T2 vertebral body (orange arrow), mild retrolisthesis of T2 on T3 (yellow arrow), mild widening of the bilateral facet joints (blue arrows). Facet joint fusion/stiffening is present at T1-T2 (red arrow). No compressive vertebral body flattening is observed.

Case 6
CIREN ID 681

2018 Honda CR-V
Striking: Large PU
Delta V: 52 km/h
PDOF: 170 deg
CDC: 06BZAW03
Seat energy: 10,807 J

Factors
Multiple impacts:
- Front w/ pass car
  (CDC: 12FREE04)

Driver
74yo Male (MAIS 3)
178 cm, 102 kg

Factors
Obesity (BMI: 32.2)
DISH
Degenerative spondylosis

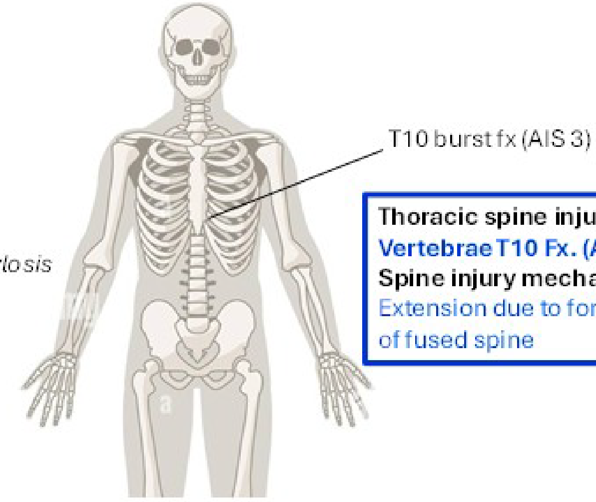

Thoracic spine injury
Vertebrae T10 Fx. (AIS 3)
Spine injury mechanism:
Extension due to forced straightening of fused spine

Kinematics: The driver moved rearward and loaded the seat. He pocketed into the seatback and straightened his stiffened spine along the seatback as it rotated. The driver moved slightly inboard with PDOF. The seat yielded. The seatback contacted the second-row seat cushion The driver likely ramped. The head restraint showed signs of occupant loading.

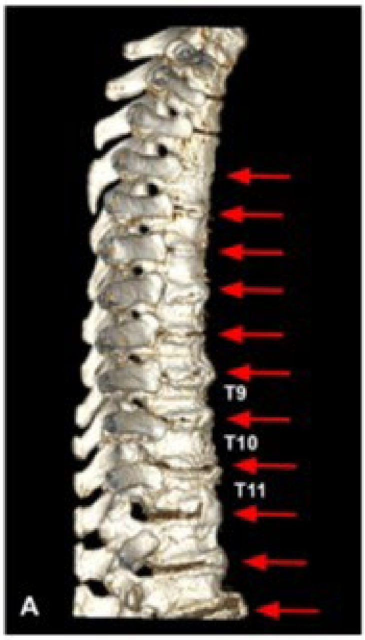

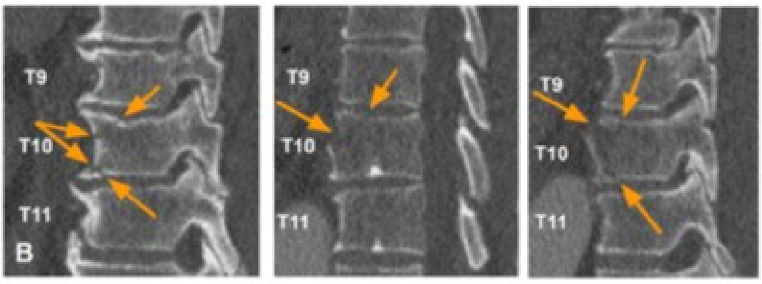

CASE 6. (A) Right lateral view of 3D reconstruction of thoracic spine CT demonstrates multilevel degenerative spondylosis and DISH, stiffening the spine, with narrowing and osteophytic bridging of the disc spaces (red arrows). **(B)** Sagittal CT images demonstrate extension fracture of the anterior aspect of the T10 vertebral body extending into the T9-T10 and T10-T11 disc spaces, with disruption of the anterior longitudinal ligament and distraction of fracture fragments (orange arrows). No compressive vertebral body flattening is observed.

Case 7

CIREN ID 704

2017 GMC Yukon XL
Striking: Pass car
Delta V: 49 km/h
EDR: 28 km/h
PDOF: 170 deg
CDC: 06BYEW03
Seat energy:
8,429 J /2,758J (EDR)

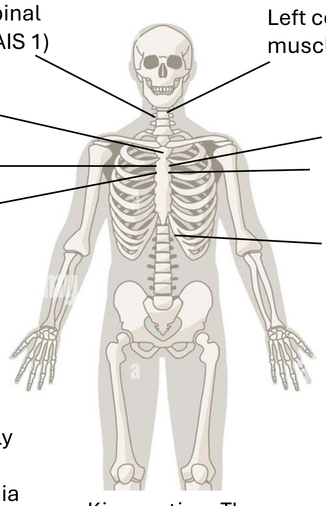

Thoracic spine injury
Vertebrae T5 (AIS 3)
Lumbar spine injury
Left vertebrae L1 (AIS 2)
Spine injury mechanism
Extension due to forced straightening of fused spine from DISH

Driver
74yo Male (MAIS 3)
180 cm, 140 kg

Factors
Obesity (BMI: 32.2)
OOP – Possibly leaning slightly inboard prior to crash
DISH, osteoporosis/osteopenia
Non-insulin dependent & blood thinner therapy

Kinematics: The occupant moved primarily rearwards, loaded the seat. The occupant's calcified spine tried to straighten along the relatively upright seatback

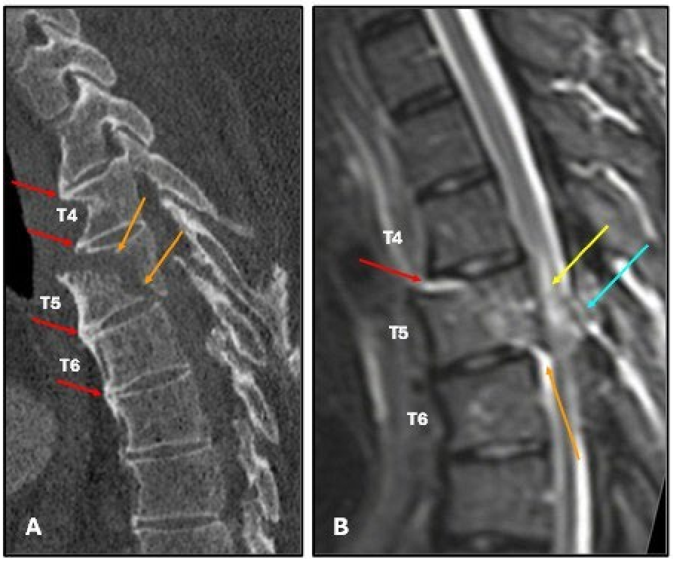

CASE 7. **(A)** Sagittal CT image demonstrates multilevel DISH, stiffening the spine, with osteophytic bridging of the disc spaces (red arrows). Oblique distracted fracture courses through the T5 vertebral body, extending into the T5-T6 disc space (orange arrows). **(B)** Sagittal STIR MR image demonstrates disruption of the anterior longitudinal ligament (red arrow), posterior longitudinal ligament with retrolisthesis of T5 on T6 (orange arrow), and the ligamentum flavum (blue arrow). These injuries result in spinal canal narrowing and spinal cord contusion (yellow arrow). No compressive vertebral body flattening nor characteristic bands of compressive bone marrow edema are identified.

Case 8

CIREN ID 709

2009 Toyota Camry
Striking: Pass car
Delta V: 95 km/h
PDOF: 200 deg
CDC: 07BLEW08
Seat energy: 19,237 J
Factors
Excess. Severity
Intrusion
Multiple impacts
- CDC: 11FYEW02

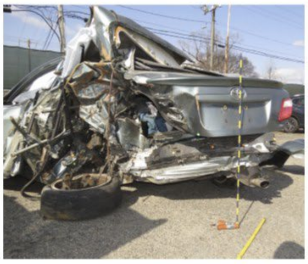

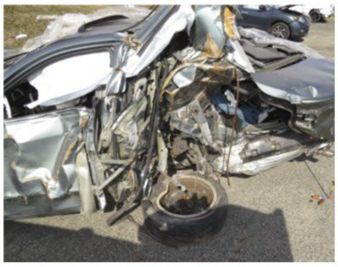

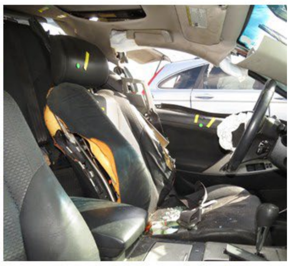

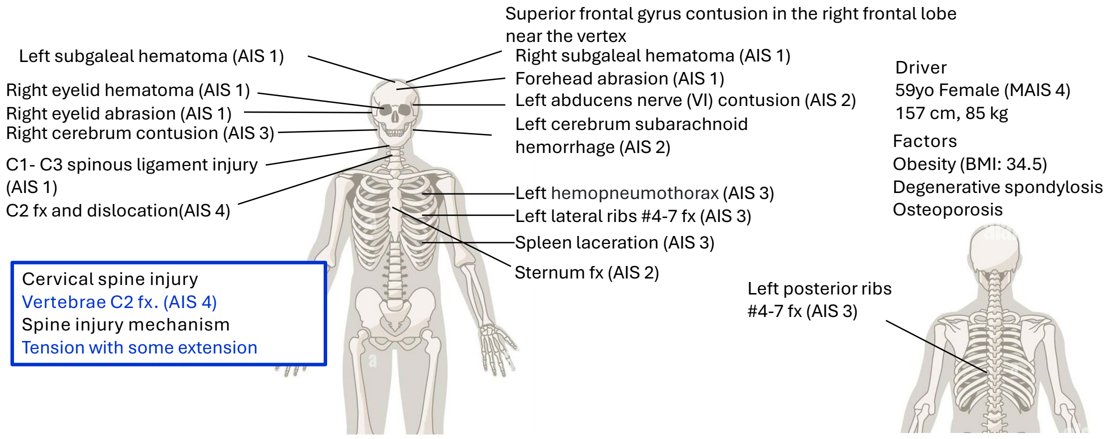

Kinematics: The driver moved rearward and outboard during the rear left corner impact resulting in a 7 o'clock PDOF. The occupant loaded the seat but the seatback was supported by 2nd row intrusion. The occupant may have ramped up the seatback and the head may have contacted the roof. The occupant then moved inboard with the vehicle counterclockwise yaw. The occupant then moved forward and to the left during the tree impact (11 o'clock PDOF). It is also possible that the degenerative change in the lower cervical spine reduced the lower C-spine mobility and increased the head rotation prior to airbag contact.

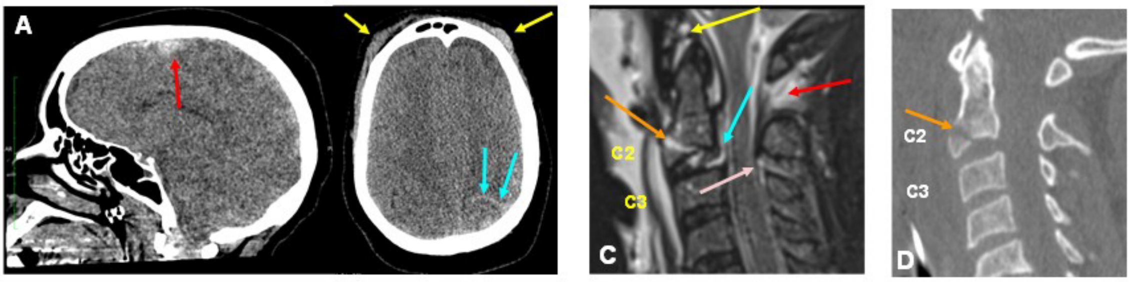

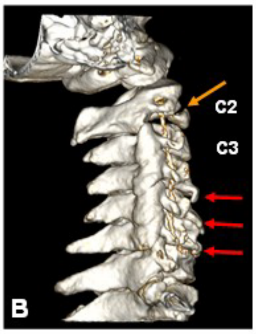

CASE 8. (A) Sagittal and axial CT image demonstrate bilateral forehead scalp hematomas (yellow arrows), superior frontal subarachnoid blood and/or contusion (red arrow), left parietal subarachnoid blood (blue arrows). **(B)** Right lateral view of 3D reconstruction of cervical spine CT demonstrates multilevel degenerative spondylosis, stiffening the spine, with narrowing and osteophytic bridging of the anterior aspects of the disc spaces (red arrows). Distracted fracture of the anteroinferior aspect of the C2 vertebral body is present (orange arrow). **(C)** Sagittal STIR MR image demonstrates disruption of the anterior longitudinal ligament and distracted fracture of the anteroinferior corner of the C2 vertebral body (orange arrow). Fluid is seen within the cleft of the fracture plane, but no characteristic band of bone marrow edema is identified within the vertebral bodies to indicate compressive loading. Disruption of the posterior longitudinal ligament (blue arrow) and the ligamentum flavum (pink arrow) are noted. Bright signal indicative of sprain/disruption is observed in the vicinity of the apical ligament (yellow arrow) and the C1-C2 interspinous ligament (red arrow). **(D)** Sagittal CT image shows distracted fracture of the anteroinferior corner of the C2 vertebral body (orange arrow). No compressive flattening of the vertebral bodies is observed. The imaging findings are consistent with extension-distraction loading to the upper cervical spine.

Case 9

CIREN ID 804

2014 Toyota Prius
Striking: Minivan
Delta V: 70 km/h
PDOF: 190 deg
CDC: 06BDEW03
Seat energy: 11,673 J

Factors
Excess. Severity
Intrusion
Multiple impacts
- CDC: 01FZEW0
- CDC: 12FLEE01

Driver
60yo Male (MAIS 3)
191 cm, 95 kg

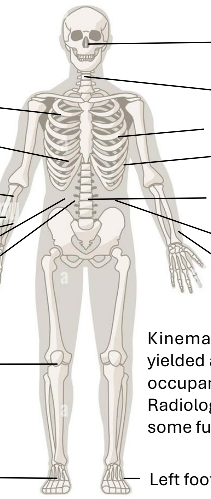

Thoracic spine injury
Central vertebrae T9 fx. (AIS 2)
Central vertebrae T10 fx. (AIS 2)
Spine injury mechanism
Flexion-distraction w/ anterior spinal column compression

Factors
Possible belt mis-routing
Osteoporosis, degenerative spondylosis

Kinematics: The occupant moved rearward and loaded the seatback. The seat yielded and the seatback rotated until it contacted the intruded 2nd row seat. The occupant then moved forward with rebound and subsequent frontal impacts. Radiology findings indicated that the shoulder belt was low on the torso, resulting in some fulcrum loading during the frontal/rebound kinematics

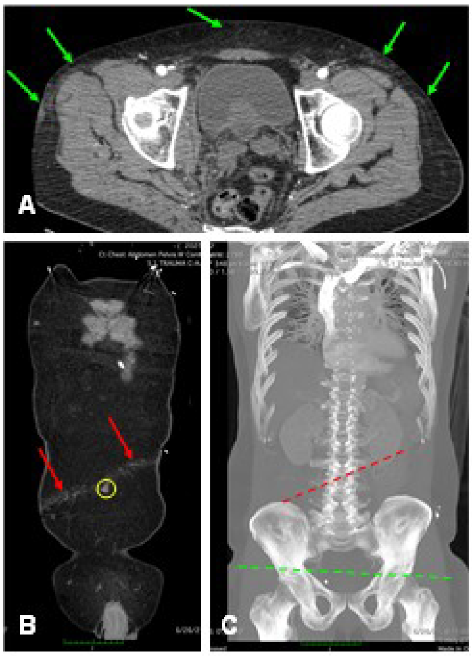

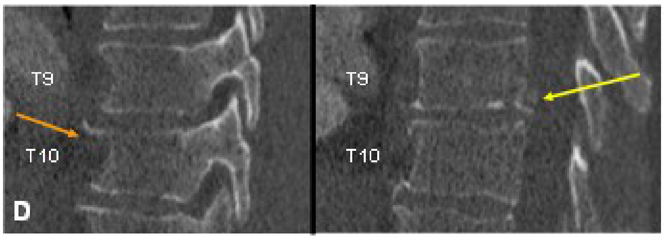

CASE 9. (A) Axial CT image demonstrates patchy areas of edema/hematoma in the subcutaneous fat anterior and anterolateral to the pelvis at the level of the hip joints (green arrows), indicative of bruising at the expected location of the lap belt. (B) Coronal CT image through the anterior wall of the chest/abdomen demonstrates diagonal band of edema/hematoma (red arrows) in the anterior subcutaneous fat at the level of the umbilicus (yellow circle), indicative of bruising from a torso belt. (C) Coronal thick MIP CT scout image demonstrates the approximate trajectories of the lap belt mark (green dashed line) and the torso belt mark (red dashed line). The torso belt mark courses lower than expected for an appropriately positioned torso belt, likely tracking below the left armpit. (D) Sagittal CT images demonstrate mild anterior wedge compression fracture of the T10 vertebral body (orange arrow) and a mildly displaced/distracted fracture of the posteroinferior corner of the T9 vertebral body (yellow arrow), consistent with hyperflexion injury.

Case 10

CIREN ID 805

2014 Toyota Prius
Striking: Minivan
Delta V: 70 km/h
PDOF: 190 deg
CDC: 06BDEW03
Seat energy: 8,356 J
Factors
Excess. Severity
Intrusion
Multiple impacts

- CDC: 01FZEW0
- CDC: 12FLEE01

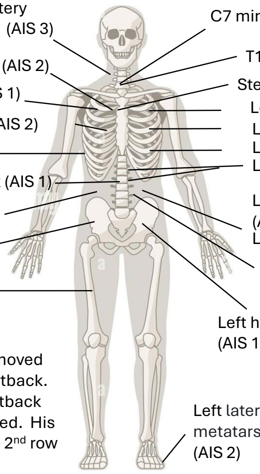

RFP
57yo Female (MAIS 4)
168 cm, 68 kg

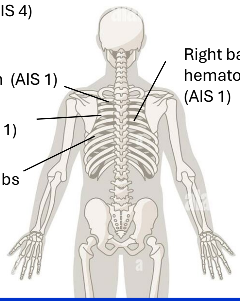

Kinematics: The occupant moved rearward and loaded the seatback. The seat yielded and the seatback rotated. The occupant ramped. His head contacted the intruded 2nd row area

Cervical/Thoracic spine injury
Vertebrae C7 fx. (AIS 2)
Vertebrae T1 fx.(AIS 2)
Spine injury mechanism:
Axial compression resulting in buckling and flexion as the back of head contacted the intruded second row seatback

CASE 10. (A) Sagittal CT image of the cervical and upper thoracic spine demonstrates mild anterior wedge compression-flexion fractures of the C7 and T1 vertebral bodies (red arrows). **(B)** Sagittal CT image of the sternum demonstrates buckle fracture of the anterior cortex of the sternal body (orange arrow).

Case 11
CIREN ID 1070

2017 BMW X3
Striking: Large PU
Delta V: 56 km/h
PDOF: 180 deg
CDC: 06BDAW04

Seat energy: 8,572 J

Factors
Excess. Severity
Intrusion
Rear tailgate intruded through cargo area

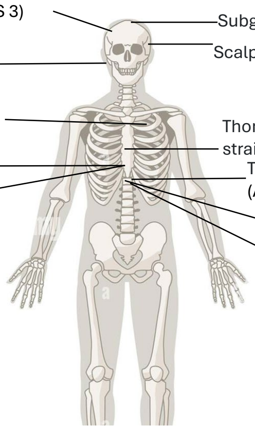

Thoracic spine injury
T3 fx (AIS 3)
T9-T10 fx (AIS 3)
Spine injury mechanism:
First: Extension at T9 level due to spine straightening of stiff spine (DISH)
Second: Compression w/flexion as the back of head contacted the rigidized 2nd row seatback and/or C-pillar at T3 level

RFP
78yo Male (MAIS 3)
175 cm,109 kg

Factors
Age, obesity,
Osteoporosis, stenosis, DISH

Kinematics: The occupant moved rearward and loaded the seatback. The fused thoracic spine fractured during spine straightening. The seat yielded and the seatback rotated. The occupant ramped. His head contact the intruded 2nd row area

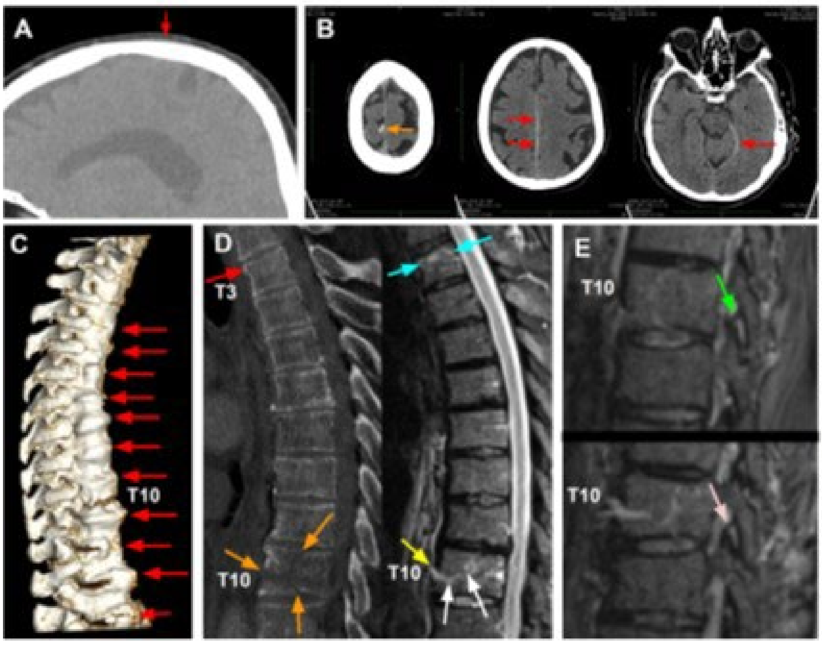

CASE 11. (A) Sagittal head CT image demonstrates tiny scalp hematoma at head vertex (red arrow). **(B)** Axial CT images show intracranial subarachnoid (orange arrow) and subdural (red arrows) blood. **(C)** Right lateral view from 3D reconstruction of thoracic spine CT demonstrates multilevel DISH, stiffening the spine, with osteophytic bridging of the disc spaces (red arrows). **(D)** Sagittal CT (left) and MR STIR (right) images demonstrate mild compression fracture of of the T3 vertebral body (red arrow) with the characteristic bright band of compressive bone marrow edema (blue arrows); T10 vertebral body extension fracture with distraction of fracture fragments (orange arrows), disruption of the anterior longitudinal ligament (yellow arrow), and fluid within the fracture clefts (white arrows). **(E)** MR images show mild widening of the bilateral T10-T11 facet joints (green and pink arrows).

Case 12
CIREN ID 98018

2018 Mercedes-Benz GLS
Striking: Car
Delta V: 30 km/h
PDOF: 180 deg
CDC: 06BDEW02

Seat energy: 2,776 J

Factors
Underride

Driver
73yo Male (MAIS 3)
BMI: 42.2
170 cm, 123 kg

Factors
Age, obesity, DISH/DS

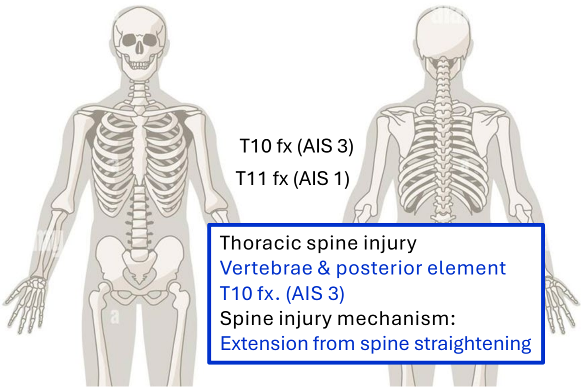

Kinematics: The occupant moved rearward and loaded the seatback. The fused thoracic spine fractured during spine straightening.

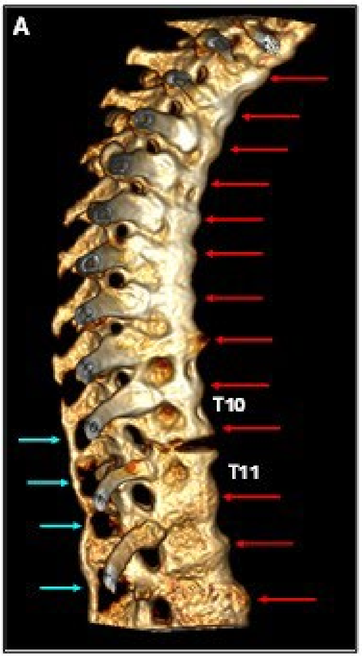

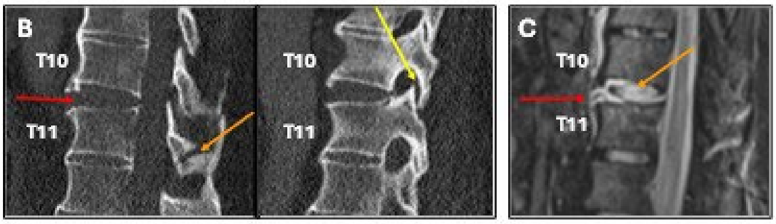

CASE 12. **(A)** Right lateral view of 3D reconstruction of thoracic spine CT demonstrates multilevel Degenerative Spondylosis and DISH, stiffening the spine, with flowing syndesmophytes bridging the disc spaces (red arrows). Ossification of the supraspinous ligament (blue arrows) further stiffens the spine. **(B)** Sagittal CT images demonstrate extension fracture through the calcified anterior longitudinal ligament (red arrow), widening of the T10-T11 disc space with slight posterior tilting of T10 relative to T11, fracture of the T11 spinous process (orange arrow), and mild T10-T11 facet joint widening (yellow arrow). **(C)** Sagittal STIR MR image shows disrupted anterior longitudinal ligament (red arrow), and abnormal bright signal (edema/blood) within the widened T10-T11 disc space (orange arrow). No compressive vertebral body flattening nor compressive bone marrow edema is observed.

Case 13

CIREN ID 980018

2023 GMC Sierra
Striking: SUV
Delta V: 34 km/h
PDOF: 190 deg
CDC: 06BYEW01
Seat energy: 2,841 J

Factors
Underride
Multiple impact
- 00UZLW02

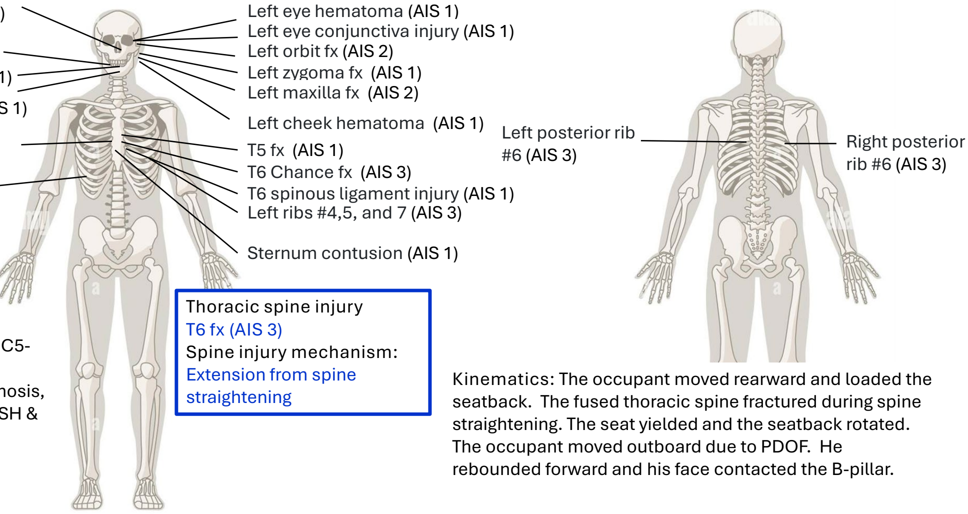

Driver
72yo Male (MAIS 3)
180 cm,98 kg

Factors
Age, obesity, prior C5-C7 joint fusion
Osteoporosis, stenosis, hyperkyphosis, DISH & degenerative spondylosis

Thoracic spine injury
T6 fx (AIS 3)
Spine injury mechanism:
Extension from spine straightening

Kinematics: The occupant moved rearward and loaded the seatback. The fused thoracic spine fractured during spine straightening. The seat yielded and the seatback rotated. The occupant moved outboard due to PDOF. He rebounded forward and his face contacted the B-pillar.

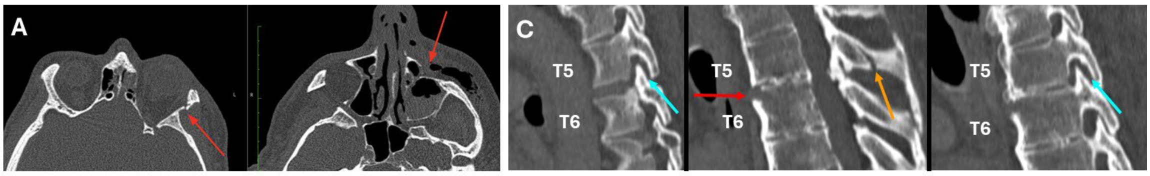

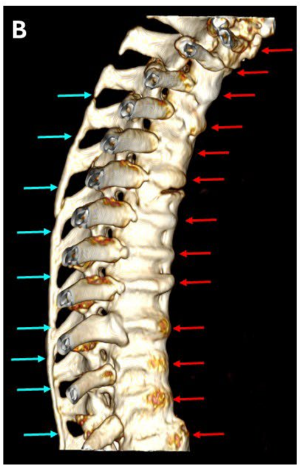

CASE 13. (A) Axial facial CT images demonstrate multiple left facial fractures, including the left orbit and the left maxillary sinus (red arrows). **(B)** Right lateral view of 3D reconstruction of thoracic spine CT demonstrates multilevel DISH and Degenerative Spondylosis, stiffening the spine, with flowing osteophytes/syndesmophytes bridging the disc spaces (red arrows). Ossification of the supraspinous ligament (blue arrows) further stiffens the spine. **(C)** Sagittal CT images demonstrate extension fracture through the calcified anterior longitudinal ligament (red arrow), widening of the anterior aspect of the T5-T6 disc space, fracture of the T5 spinous process (orange arrow), and widening of the bilateral T5-T6 facet joints (blue arrows). No compressive vertebral body flattening is observed.

Case 14

CIREN ID 980021

2017 Infiniti Q50
Striking: Car
Delta V: 79 km/h
PDOF: 190 deg
CDC: 06BYEW08;
Seat energy: 15,964 J

Factors
Crash severity
Underride
Multiple impact

- 99U99999

Driver
51yo Male (MAIS 4)
173 cm,102 kg

Factors
Severe intrusion

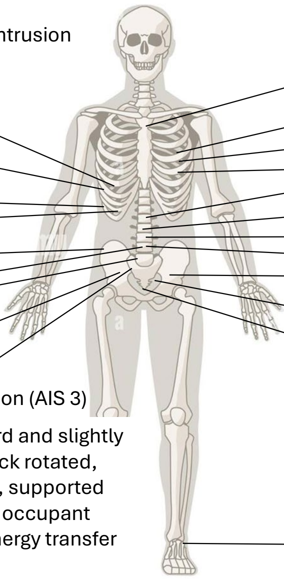

Kinematics: The occupant moved rearward and slightly outboard. The seat yielded and the seatback rotated, however, the second-row intrusion limited, supported and bolstered with seatback rotation. The occupant ramped up into the roof structures. The energy transfer to the seat was exceedingly severe.

Thoracic spine injury
Left vertebrae T3 (AIS 2)
Spine injury mechanism:
Compression-flexion (buckling)

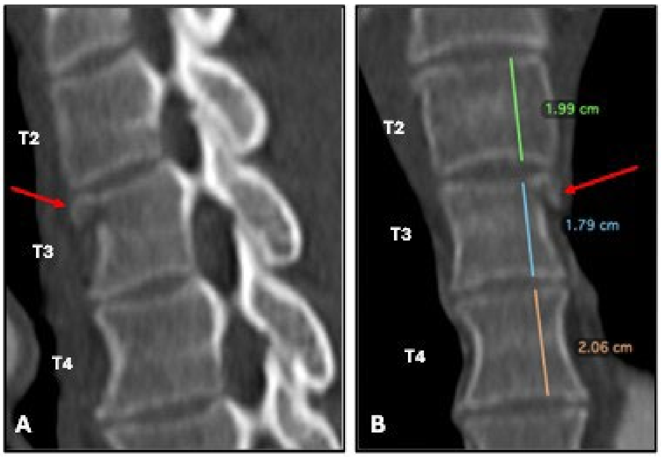

CASE 14. (A) Sagittal CT image demonstrates fracture of the anterosuperior corner of the T3 vertebral body (red arrow). **(B)** Coronal CT image demonstrates fracture extending to the left superior aspect of the vertebral body (red arrow) with ~10% loss of vertebral body height, indicative of compressive loading to the anterior spinal column.

Case 15
CIREN ID 980038

2018 Subaru XV Crosstrek
Striking: Pass car
Delta V: 54 km/h
PDOF: 170 deg
CDC: 06BDEW04
Seat energy: 6,801 J

Factors
Crash severty

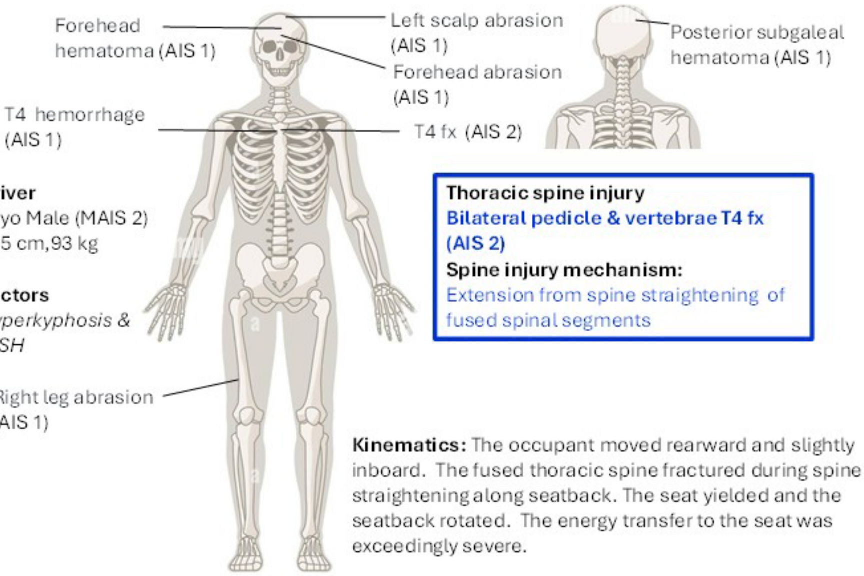

Driver
53yo Male (MAIS 2)
185 cm, 93 kg

Factors
Hyperkyphosis & DISH

Thoracic spine injury
Bilateral pedicle & vertebrae T4 fx (AIS 2)
Spine injury mechanism:
Extension from spine straightening of fused spinal segments

Kinematics: The occupant moved rearward and slightly inboard. The fused thoracic spine fractured during spine straightening along seatback. The seat yielded and the seatback rotated. The energy transfer to the seat was exceedingly severe.

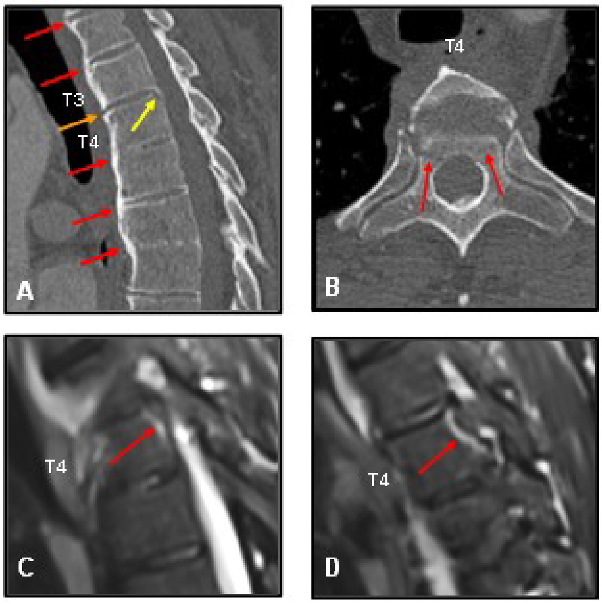

CASE 15. (A) Sagittal CT image demonstrates fracture of the posterosuperior corner of the T4 vertebral body (yellow arrow) and fracture through the ossified T3-T4 anterior longitudinal ligament (orange arrow). Multilevel DISH stiffens the spine, with flowing osteophytes bridging the disc spaces (red arrows). (B) Axial CT image demonstrates nondisplaced fractures of the bilateral T4 pedicles (red arrows). (C, D) Sagittal STIR MR images demonstrate bright fluid within the clefts of the bilateral T4 pedicle fractures (red arrows). No compressive vertebral body flattening nor characteristic bright bands of compressive bone marrow edema are identified.

Case 16

CIREN ID 980076

2015 Chevrolet Malibu
Striking: Pass car
Delta V: 76 km/h
PDOF: 170 deg
CDC: 06BREE06
Seat energy: 16,223J

Factors
Crash severity
Multiple impact
- 09LPEW012

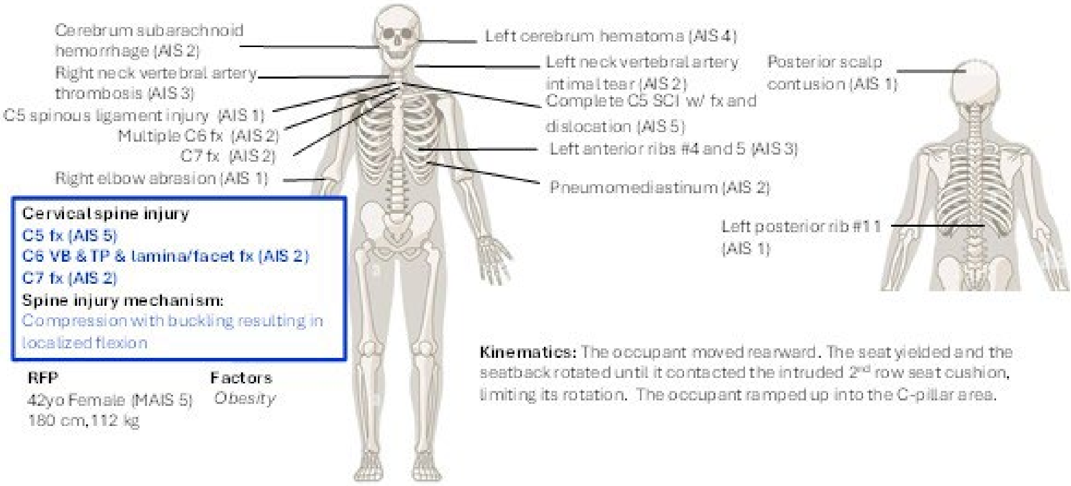

Cervical spine injury
C5 fx (AIS 5)
C6 VB & TP & lamina/facet fx (AIS 2)
C7 fx (AIS 2)
Spine injury mechanism:
Compression with buckling resulting in localized flexion

RFP
42yo Female (MAIS 5)
180 cm, 112 kg

Factors
Obesity

Kinematics: The occupant moved rearward. The seat yielded and the seatback rotated until it contacted the intruded 2nd row seat cushion, limiting its rotation. The occupant ramped up into the C-pillar area.

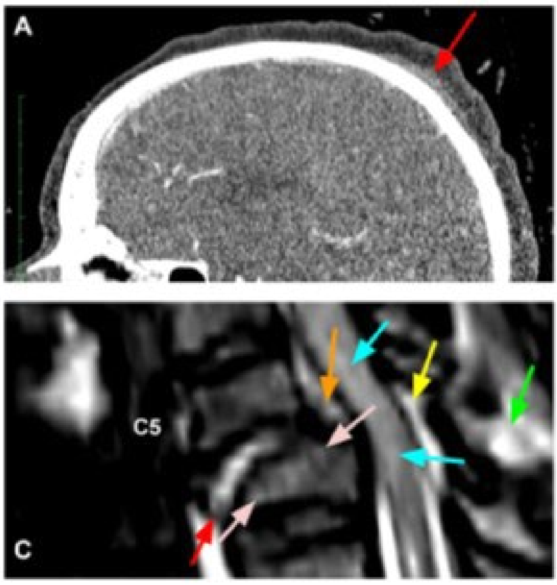

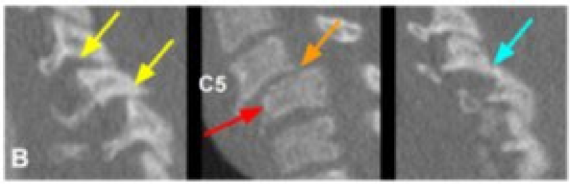

CASE 16. (A) Sagittal CT image demonstrates scalp hematoma posterior to head vertex (red arrow). **(B)** Sagittal CT images demonstrate anterior wedge compression fracture of the C6 vertebral body (red arrow), anterolisthesis of C5 on C6 (orange arrow), jumped/dislocated (blue arrow) and subluxed (yellow arrows) facet joints, consistent with localized lower cervical spinal compression-flexion loading following compressive spinal buckling. **(C)** Sagittal T2-weighted MR image demonstrates disruption of the anterior longitudinal ligament (red arrow), posterior longitudinal ligament (orange arrow), ligamentum flavum (yellow arrow), and interspinous/supraspinous ligaments (green arrow). Bright signal within the spinal cord is indicative of spinal cord contusion (blue arrows). Band of bright bone marrow signal adjacent to the compressed C6 superior vertebral body endplate (pink arrows) is characteristic of compressive vertebral body loading.

Case 17-18

CIREN ID 980090-91

2014 Chevrolet Impala LT
Striking: SUV
Delta V: 71 kmph
PDOF: 180 deg
CDC: 06BDEW06

Seat energy:
Driver: 12,009 J
RFP: 11,883 J

Factors
Crash severity
Multiple impacts
- Minor rear
    - 06B9MW01

Driver
73yo Male (MAIS 4)
175 cm/95 kg

Factors
Age, obesity
Prior cervical laminectomy
Thoracic aorta disease
Osteoporosis, stenosis & DISH

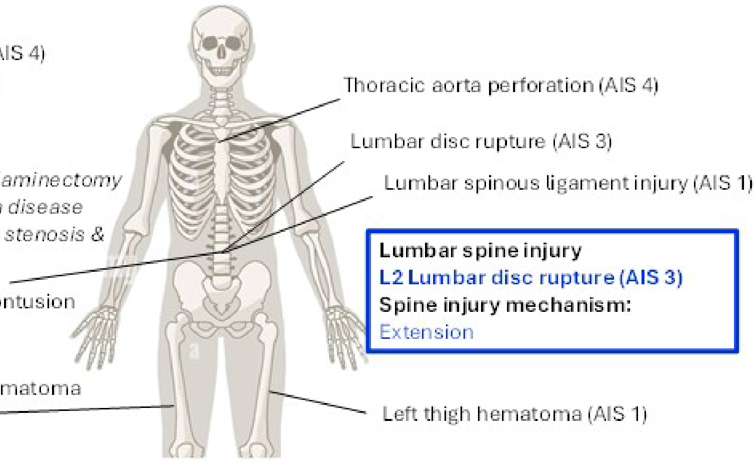

Lumbar spine injury
L2 Lumbar disc rupture (AIS 3)
Spine injury mechanism:
Extension

Kinematics: During the first and most severe rear impact, the occupant moved rearward. The seat yielded and the seatback rotated until it was supported by the 2nd row seat cushion. The energy transfer to the seat was exceedingly severe. Seatback-2nd row seat cushion impact resulted in loading in the lumbar area and likely detachment of the riser. The 2nd rear impact was minor. However, the seatback was previously reclined.

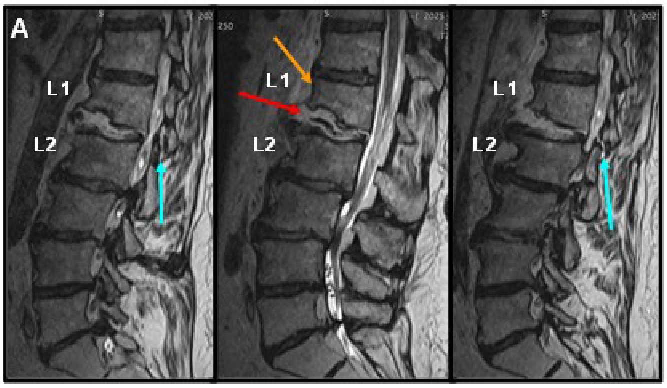

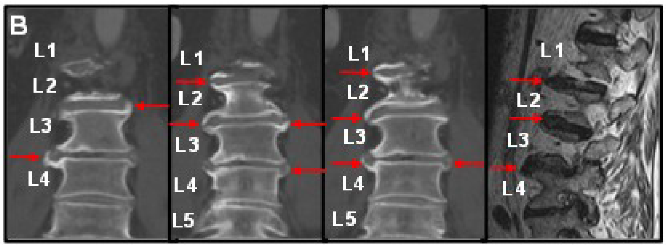

CASE 17. (A) Sagittal T2-weighted MR images demonstrate disruption of the anterior longitudinal ligament, widening of the disc space at L1-L2 (red arrow), and mild widening of the bilateral L1-L2 facet joints (blue arrow). Anterior wedge compression fracture of the L1 vertebral body (orange arrow) appears chronic, given the absence of compressive bone marrow edema. **(B)** Coronal CT images and sagittal MR image demonstrate multilevel DISH, stiffening the spine, with flowing osteophytes bridging the disc spaces (red arrows)

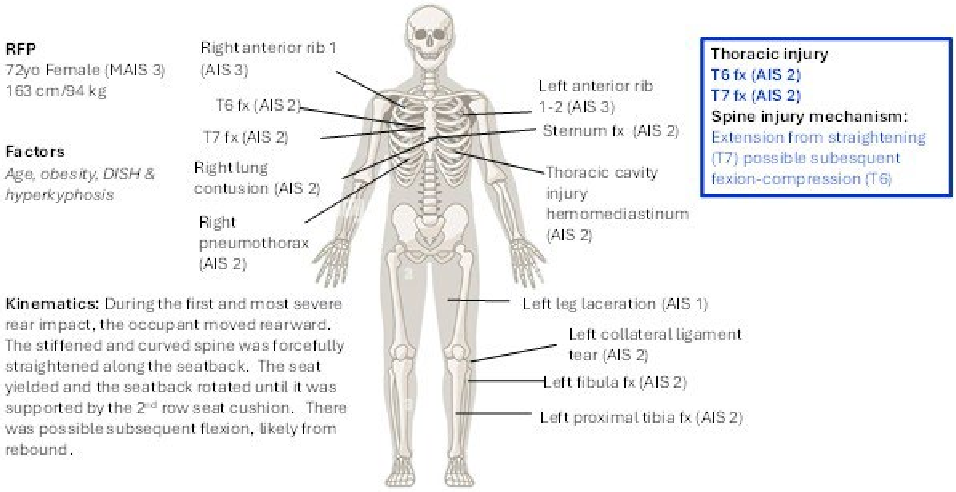

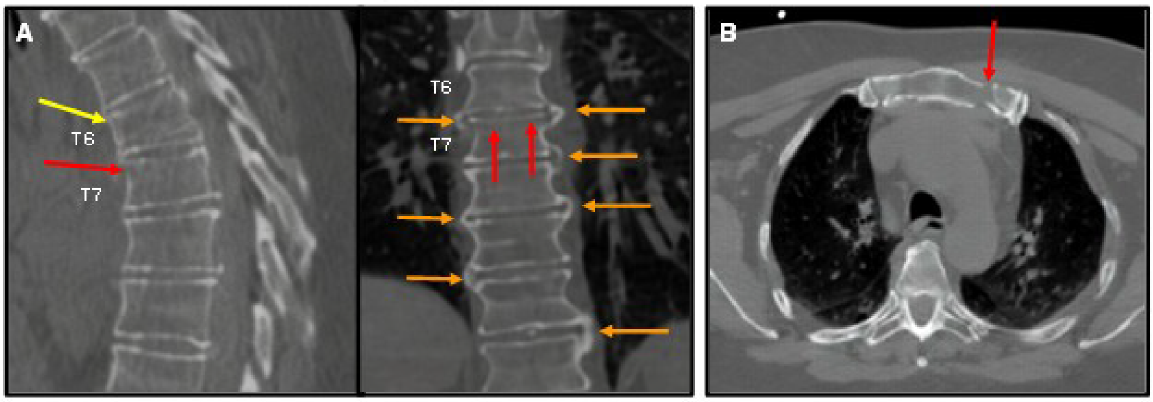

CASE 18. (A) Sagittal (left) and coronal (right) CT images demonstrate mildly distracted fracture through the superior aspect of the T7 vertebral body and the associated anterior longitudinal ligament (red arrows). Mild anterior wedge compression fracture of the T6 vertebral body (yellow arrow)is also present. Multilevel DISH stiffens the spine, with flowing osteophytes bridging the disc spaces (orange arrows). (B) Axial CT image at the level of the upper chest demonstrates fracture through the left side of the sternum (red arrow).

Case 19

CIREN ID 980114

2024 Chevrolet Blazer
Striking: Minivan
Delta V: 30 kmph
PDOF: 180 deg
CDC: 06BYEW02
Seat energy: 1,783 J

Factors
Multiple impacts
- 02RPEW01

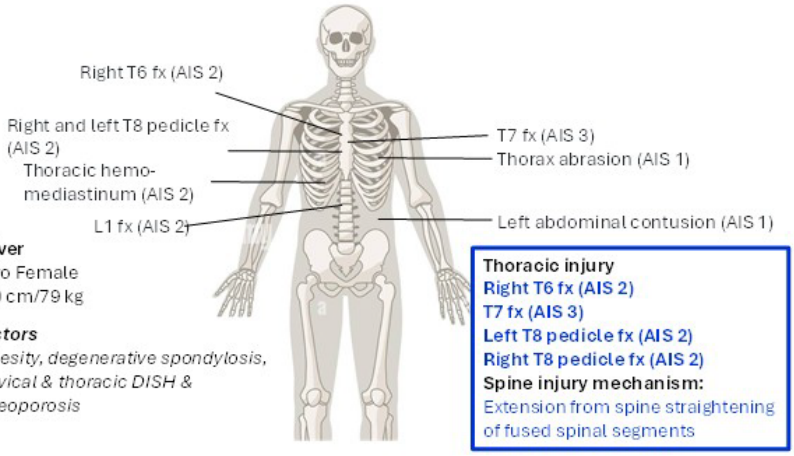

Driver
62yo Female
160 cm/79 kg

Factors
Obesity, degenerative spondylosis, cervical & thoracic DISH & osteoporosis

Thoracic injury
Right T6 fx (AIS 2)
T7 fx (AIS 3)
Left T8 pedicle fx (AIS 2)
Right T8 pedicle fx (AIS 2)
Spine injury mechanism:
Extension from spine straightening of fused spinal segments

Kinematics: The occupant moved rearward. The fused thoracic spine fractured during spine straightening along seatback. The seat yielded and the seatback rotated.

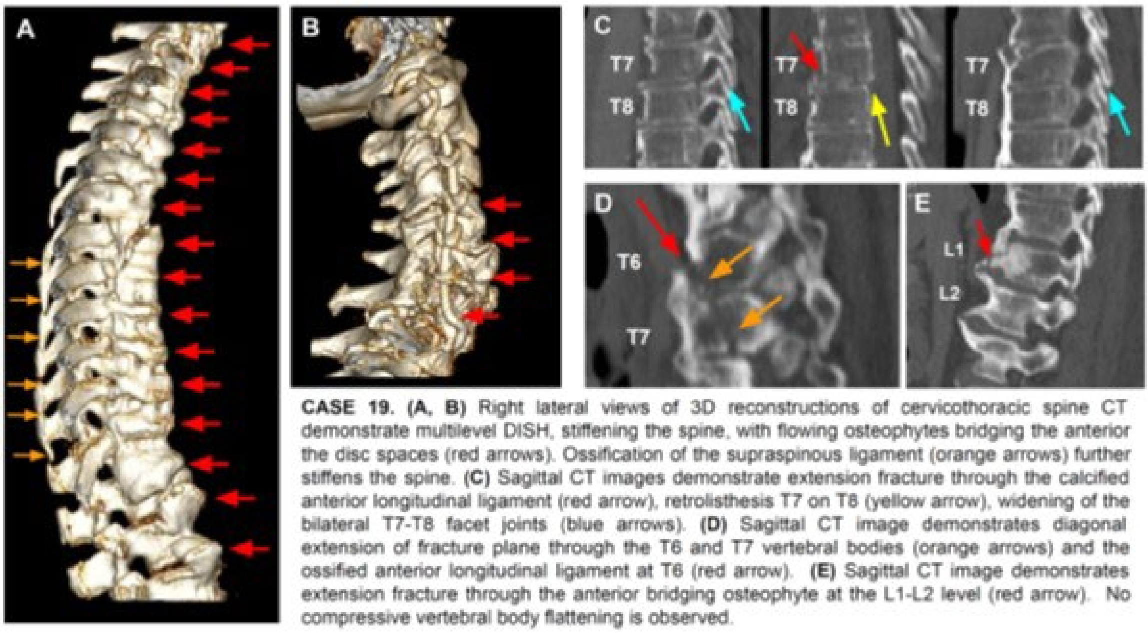

CASE 19. (A, B) Right lateral views of 3D reconstructions of cervicothoracic spine CT demonstrate multilevel DISH, stiffening the spine, with flowing osteophytes bridging the anterior the disc spaces (red arrows). Ossification of the supraspinous ligament (orange arrows) further stiffens the spine. **(C)** Sagittal CT images demonstrate extension fracture through the calcified anterior longitudinal ligament (red arrow), retrolisthesis T7 on T8 (yellow arrow), widening of the bilateral T7-T8 facet joints (blue arrows). **(D)** Sagittal CT image demonstrates diagonal extension of fracture plane through the T6 and T7 vertebral bodies (orange arrows) and the ossified anterior longitudinal ligament at T6 (red arrow). **(E)** Sagittal CT image demonstrates extension fracture through the anterior bridging osteophyte at the L1-L2 level (red arrow). No compressive vertebral body flattening is observed.

Case 20
CIREN ID 980121

2024 Toyota RAV4
Striking: Car
Delta V: 49 km/h
PDOF: 190 deg
06BYEW03

Seat energy: 6,804 J

Factors
Multiple impacts
- 11LDES01

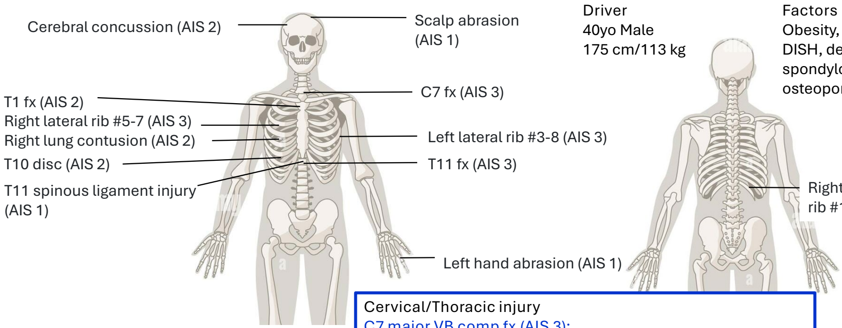

Driver
40yo Male
175 cm/113 kg

Factors
Obesity,
DISH, degenerative spondylosis & osteoporosis

Kinematics: The occupant moved rearward and slightly outboard. The fused thoracic spine fractured during spine straightening along seatback. The seat yielded and the seatback rotated. The occupant ramped. His head contacted the 2nd row area

Cervical/Thoracic injury
C7 major VB comp fx (AIS 3);
T1 minor VB fx (AIS 2)
T10 disc injury (AIS 2)
T11 VB comp fx (AIS 3)
Spine injury mechanism:
Extension from spine straightening of fused spinal segments (T10-T11)
Compression w/flexion (C7-T1)

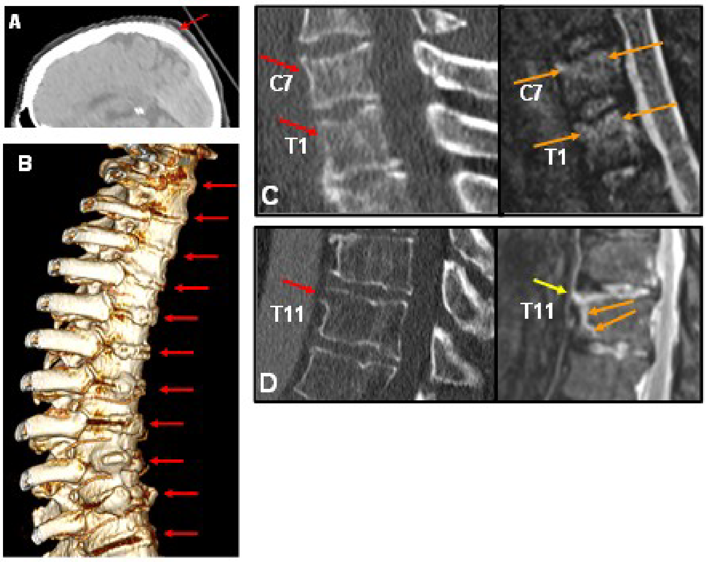

CASE 20. (A) Sagittal head CT image demonstrates scalp hematoma posterior to the head vertex (red arrow). **(B)** Right lateral view from 3D reconstruction of thoracic spine CT demonstrates multilevel degenerative spondylosis and DISH, stiffening the spine, with osteophytic narrowing/bridging of the disc spaces (red arrows). **(C)** Sagittal CT (left) and MR STIR (right) images demonstrate mild compression fractures of the C7 and T1 vertebral bodies (red arrows) with characteristic bright bands of compressive bone marrow edema (orange arrows). **(D)** Sagittal CT (left) and MR STIR (right) images demonstrate T11 vertebral body extension fracture with distraction of fracture fragments (red arrow), disruption of the anterior longitudinal ligament (yellow arrow), and fluid within the fracture clefts (orange arrows). No compressive vertebral body flattening nor compressive bone marrowedema is identified.

Case 21

CIREN ID 980150

2015 Audi A3
Striking: SUV
Delta V: 41 km/h
PDOF: 180 deg
06BDEW06

Seat energy:
2,993 J

Factors
Multiple impacts
- 12FDEW02

Seat moved rearward & seatback reclined for extrication

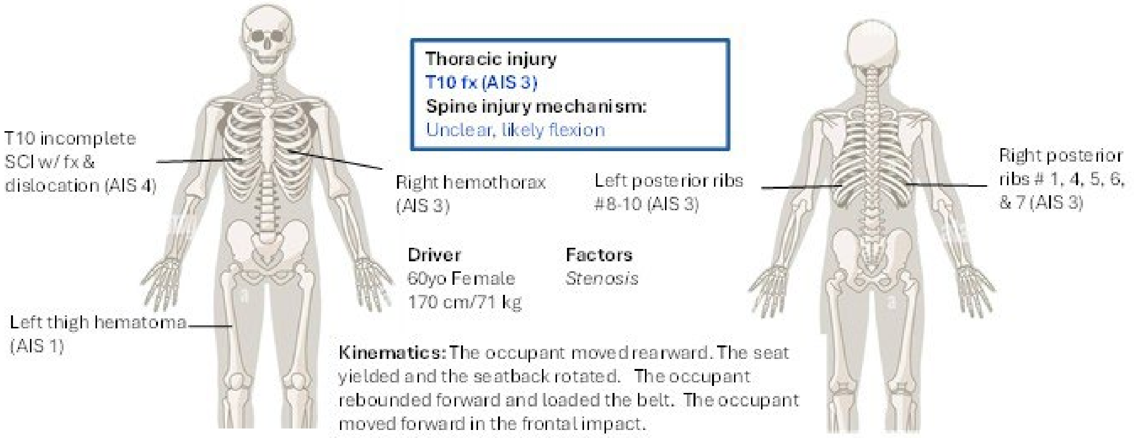

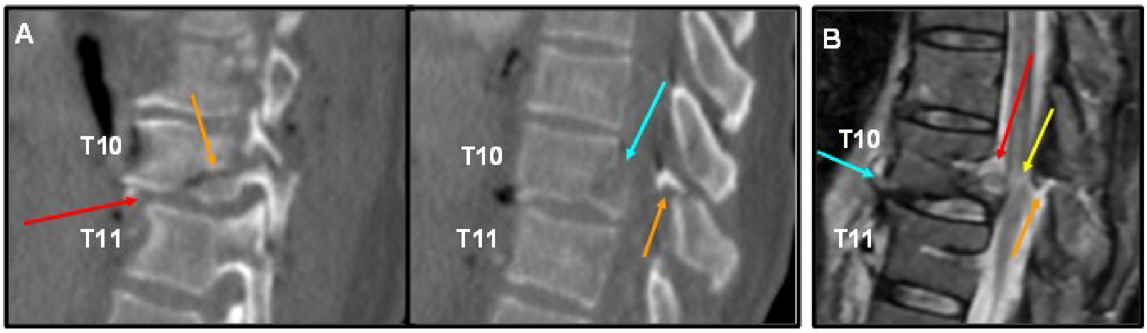

CASE 21. (A) Sagittal CT images demonstrate fracture through the posteroinferior aspect of the T10 vertebral body extending into the facet columns and spinous process (orange arrows). Anterolisthesis of T10 on T11 is present (red arrow) with distraction of the fracture fragment at the posteroinferior corner of the T10 vertebral body (blue arrow). **(B)** Sagittal MR STIR image demonstrates distraction of fracture fragments and disruption of the posterior longitudinal ligament (red arrow), disruption of the anterior longitudinal ligament (blue arrow), ligamentum flavum (orange arrow), and narrowing of the spinal canal with bright spinal cord edema/contusion (yellow arrow). No vertebral compressive flattening nor compressive bone marrow edema is identified.

Case 22

CIREN ID 980340

2014 Lexus IS 250
Striking: Large PU
Delta V: 80 kmph
PDOF: 180 deg
CDC: 06BDAW06

Seat energy: 11,716 J

Factors
Multiple impacts
- 12FDEW02
- 01FYEW01

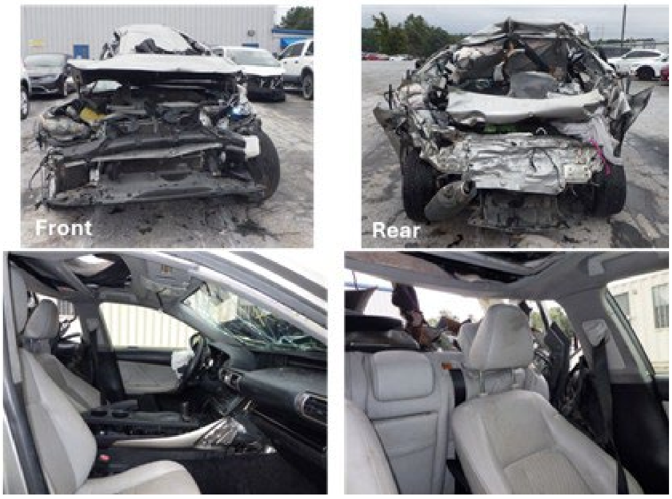

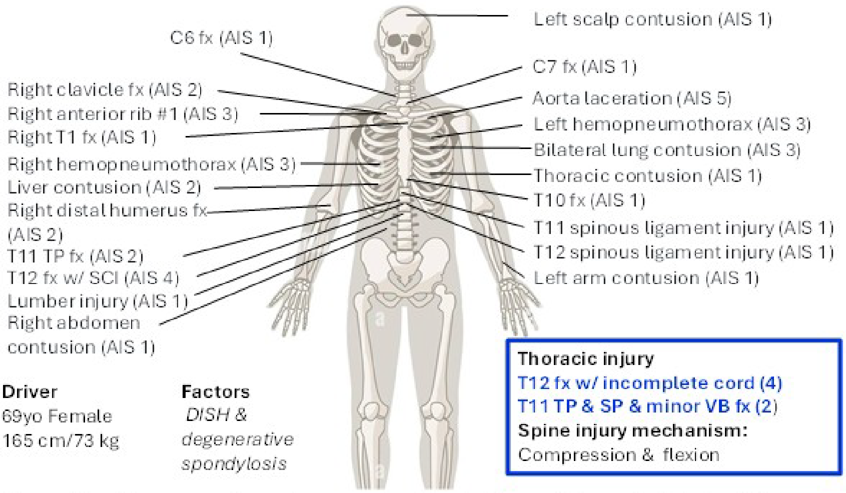

Kinematics: The occupant moved rearward and loaded the seat. The seat yielded and the seatback rotated. Intrusion occurred early. The second row intruded, supported and loaded the driver seat.

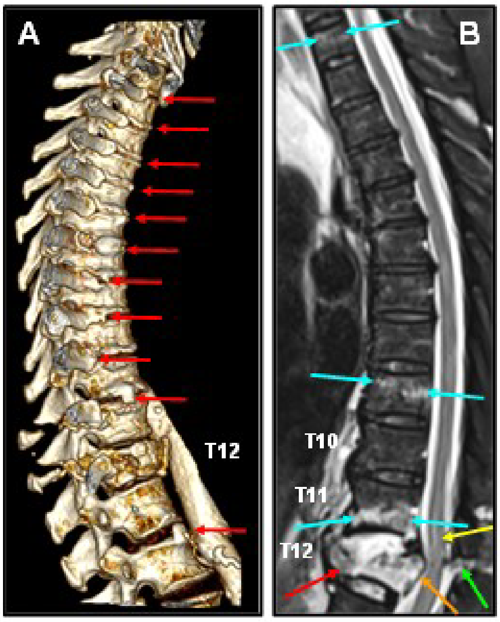

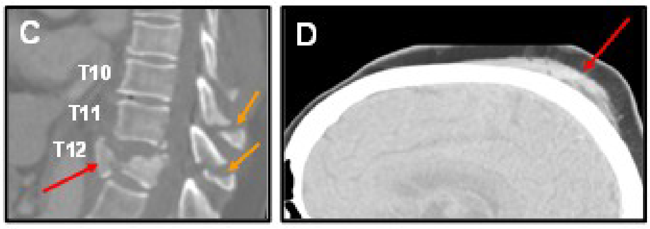

CASE 22. (A) Right lateral view from 3D reconstruction of thoracic spine CT demonstrates multilevel degenerative spondylosis and DISH, stiffening the spine, with osteophytic narrowing/bridging of the of the disc spaces (red arrows). (B) Sagittal STIR MR image demonstrates severe burst compression fracture of T12 vertebral body with retropulsion of fracture fragments into the spinal canal (orange arrow), causing spinal cord compression and bright spinal cord edema/contusion (yellow arrow). Disruption of the ligamentum flavum and interspinous ligament are also present (green arrow). Characteristic bright bands of compressive bone marrow edema without frank flattening of vertebral bodies are noted at multiple levels (blue arrows). (C) Sagittal CT image shows burst compression fracture of the T12 vertebral body and distracted fractures of the T10 and T11 spinous processes, indicative of compression-flexion loading. (D) Sagittal head CT image demonstrates scalp hematoma posterior to the head vertex (red arrow).